Combinatorial strategies using CRISPR/Cas9 for gene mutagenesis in adult mice

Avery C. Hunker

A dissertation

submitted in partial fulfillment of the

requirements for the degree of

Doctor of Philosophy

University of Washington

2019

Reading Committee:

Larry S. Zweifel, Chair

Sheri J. Mizumori

G. Stanley McKnight

Program Authorized to Offer Degree:

Pharmacology

University of Washington

ABSTRACT

Combinatorial strategies using CRISPR/Cas9 for gene mutagenesis in adult mice

Avery C. Hunker

Chair of the Supervisory Committee:

Larry Zweifel

Department of Pharmacology

A major challenge to understanding how genes modulate complex behaviors is the inability to restrict genetic manipulations to defined cell populations or circuits. To circumvent this, we created a simple strategy for limiting gene knockout to specific cell populations using a viral-mediated, conditional CRISPR/SaCas9 system in combination with intersectional genetic strategies. A small single guide RNA (sgRNA) directs *Staphylococcus aureus* CRISPR-associated protein (SaCas9) to unique sites on DNA in a Cre-dependent manner resulting in double strand breaks and gene mutagenesis *in vivo*. To validate this technique we targeted nine different genes of diverse function in distinct cell types in mice and performed an array of analyses to confirm gene mutagenesis and subsequent protein loss, including IHC, cell-type specific DNA sequencing, electrophysiology, Western blots, and behavior. We show that these vectors are as efficient as conventional conditional gene knockout and provide a viable alternative to complex genetic crosses. This strategy provides additional benefits of

targeting gene mutagenesis to cell types previously difficult to isolate, and the ability to target genes in specific neural projections for gene inactivation. Our studies illuminate AAV1-CMV-FLEX-SaCas9-U6-sgRNA as a valuable tool for rapid, efficient and robust analysis of gene function.

TABLE OF CONTENTS

CHAPTER 1: BACKGROUND

Introduction

The Clustered Regularly Interspaced Short Palindromic Repeats (CRISPR) and CRISPR-associated (Cas) proteins were first identified by microbiologists as a series of short repeat sequences in *Escherichia coli*. Metagenomic analyses, bacterial survival assays, and meticulous scientists facilitated our understanding of the mechanism of action of CRISPR/Cas9 in bacterial adaptive immunity. With the realization that this system can be exploited for gene mutagenesis in eukaryotes, CRISPR/Cas9 has emerged as a powerful genetic tool in studies ranging from basic research to translational medicine. Due to its wide array of applications, high specificity, and general simplicity, CRISPR/Cas9 may arguably be one of the greatest scientific discoveries of the century.

CRISPR/Cas9 and Adaptive Bacterial Immunity

Bacteria and archaea use CRISPR/Cas systems to retain memories of past foreign invasions to prevent future infections. This process of adaptive immunity can be split into three phases: adaptation, expression, and interference (Makarova and Koonin, 2015). The adaptation phase consists of the recognition and integration of foreign DNA into the CRISPR locus. Cas proteins bind DNA from incoming bacteriophage or viruses, cleave it into fragments, and inserts small (20-22bp) DNA pieces (spacers) into the hypervariable region (leader end) of the CRISPR locus in its own genome. The exact

mechanism of this process is not well understood, but it is thought to involve Cas1 and Cas2 proteins in most systems (Wilkinson et al., 2019).

The second phase involves the expression of small RNAs from the CRISPR locus (Ishino et al., 2018). The repeat sequences within the CRISPR locus are known as trans-activating CRISPR RNA (tracrRNA), and act as a scaffold for Cas9, while the spacers, CRISPR RNA (crRNA), specifically matches regions on foreign DNA called proto-spacers. After transcription of the CRISPR locus, the pre-RNA is cleaved by RNase III into the crRNA and tracrRNA. The processed RNA and Cas9 protein form a ribonucleoprotein (RNP) complex that targets and cleaves intruding DNA, effectively inhibiting reoccurring infection (Ishino et al., 2018; Jiang et al., 2015; Jinek et al., 2012).

Most CRISPR/Cas systems can be divided into two classes based on the Cas proteins necessary for the interference phase (Makarova and Koonin, 2015). Type I systems use multiple Cas proteins that form a complex to recognize and cleave foreign DNA, while Type II systems use a single Cas protein (typically Cas9). Cas proteins recognize PAM (proto-spacer adjacent motifs) sequences on foreign DNA and cleave the DNA 3bp upstream of PAM (Ran et al., 2015; Ran et al., 2013). Cleverly, PAM sequences are not inserted into the CRISPR locus, preventing Cas proteins from recognizing sequences on its own DNA, thereby blocking self-DNA cleavage. Unlike eukaryotic adaptive immunity, incorporating foreign DNA into the genome via CRISPR/Cas allows memories of past infections to be transferred to future generations (Ishino et al., 2018).

The discovery of CRISPR/Cas9

The locus comprising the CRISPR array was first discovered in 1987 while researching potential genes involved in phosphate metabolism in *E. coli* (Ishino et al., 1987). When sequencing the *iap* gene, Ishino et al. observed repeated sequences separated by short pieces of DNA but did not understand the function of the locus. A few years later in the early 1990s, a similar locus containing repeat sequences was discovered in archaea, suggesting evolutionary conservation (Mojica et al., 2000). Within the field of microbiology, more bacteria and almost all archaea were found to have similar arrays of repeat sequences, and in 2002 the name “CRISPR” was suggested and accepted in the field (Jansen et al., 2002).

Nearly two decades after the discovery of the locus, three papers were published independently that made key connections and observations of the locus, while also proposing potential mechanisms in bacterial adaptive immunity. First, spacer regions of the CRISPR locus in bacteria were found to match the DNA of bacteriophages and plasmids (Mojica et al., 2005; Pourcel et al., 2005). Second, a positive correlation between the number of spacers with phage origin and the ability for phage infection resistance was observed (Bolotin et al., 2005). Furthermore, these studies recognized Cas proteins as binding to some of the non-translated RNA elements, suggesting they were also potentially involved in this mechanism.

To test whether the CRISPR locus and Cas proteins play a role in bacterial immunity, the Horvath lab generated phage-resistant mutants by subjecting a wildtype naïve *S. thermophilus* strain of bacteria to two different bacteriophages (Barrangou et al., 2007). Specific *Cas* genes within the phage-resistant mutant *S. thermophilus* were inactivated which consequently resulted in a loss of phage-resistance. Inspection of the

CRISPR locus in each of the mutants revealed the addition of short sequences that were homologous to the DNA of the bacteriophage, suggesting the ability of foreign DNA to be incorporated into the locus. This was further validated by a metagenomic analysis of sequences in archaea that also indicated rapid changes at the CRISPR locus (Andersson and Banfield, 2008).

To resolve the exact mechanism of Cas proteins, a series of experiments were performed that introduced a plasmid containing bacteriophage DNA into *S. thermophilus* to mimic bacteriophage infections (Garneau et al., 2010*)*. After transfection, plasmid destabilization and integration of small pieces of plasmid were discovered at the CRISPR locus in the genome of *S. thermophilus*. Southern hybridizations of double stranded DNA from bacteriophage infecting *S. thermophilus* revealed Cas9 cleaves double stranded DNA within the proto-spacer region (just upstream of the PAM sequence).

After it was established that Cas9 can produce precise DNA double strand breaks *in vivo*, the potential of CRISPR/Cas in genome editing was recognized and the field quickly expanded. To simplify the system for research use, a short linker fused the crRNA and tracrRNA system into the single guide RNA (sgRNA) (Jinek et al., 2012). To determine the necessity of components in the CRISPR/Cas system, HEK293FT cells were transfected with different combinations of components from the CRISPR locus including SpRNase III (for processing of pre-crRNA), crRNA, tracrRNA and *Streptococcus pyogenes* Cas9 (SpCas9) (Cong et al., 2013). Targeted mutagenesis was achieved in the absence of SpRNase III, deducing this was due to the presence of endogenous mammalian RNase III. Nuclear localization sequences (NLS) were added

to both the N- and C-terminus of the mammalian codon-optimized SpCas9 to increase the ability for SpCas9 to enter and remain in the nucleus (Cong et al., 2013; Mali et al., 2013). These modifications streamlined, simplified, and increased efficacy of the system, and SpCas9 and its affiliated sgRNA are now standards in the CRISPR/Cas genome editing field in eukaryotes.

Cas9 Structure and Mechanism of DNA Cleavage

Recent crystallography studies of SpCas9 complexed with its sgRNA have provided insight into the structure-function relationship of the protein (Nishimasu et al., 2014). SpCas9 is divided into two functionally diverse lobes that are connected by a bridge helix. The recognition (REC) lobe consists of residues that interact with the sgRNA and target DNA strand, while the nuclease (NUC) lobe executes the DNA cleavage. The NUC lobe contains two nuclease domains, the wedge (WED) domain and the PAM interacting (PI) domain. The RuvC nuclease domain cleaves the non-target DNA strand, while the HNH nuclease domain cleaves the target strand (Jiang and Doudna, 2017).

Residues in the REC lobe of SpCas9 form hydrogen bonds with bases in both the sgRNA and target DNA. SpCas9 binds to three hairpin loops that form due to the secondary structure of the sgRNA. The crRNA, which is the 5’ end of the sgRNA complementary to the intended target region, is 20-21bp in length, and can be divided into the seed region and distal region (Jiang and Doudna, 2017; Sternberg et al., 2014). The seed region comprises the ~7 bases that binds directly upstream of the PAM site on the target DNA. The distal region is the most 5’ end of the sgRNA. After Cas9 binds

to the sgRNA to form a complex, the ribonucleoprotein (RNP) scans the DNA for PAM sites. Without the presence of a PAM, the RNP quickly dissociates from the DNA, allowing Cas9 to continue scanning the DNA (Sternberg et al., 2014). When a PAM site is detected, the WED domain forms multiple hydrogen bonds with the sugar phosphate backbone, slowing the off kinetics of the RNP complex, and separating local DNA base pairing. These events permit the sgRNA to come in close contact with the proto-spacer, while the non-target strand forms the R-loop (Fuchsbauer et al., 2019; Mekler et al., 2017).

Due to the proximity of the sgRNA seed region directly next to the PAM site, perfect complementation of the seed region with the target DNA is required to provide thermal energy to unwind the target DNA (Sternberg et al., 2014). Only complete binding of the sgRNA to the target sequence produces a conformational shift in Cas9, which in turn unwinds the DNA. This brings the target and non-target strands close to the HNH and RuvC nuclease domains, respectively, producing double strand breaks and the activation of either homologous directed repair (HDR) or the error-prone non-homologous end joining (NHEJ) cell repair pathways.

AAV-mediated in vivo genome editing

CRISPR/Cas9 has emerged as a technique to rapidly generate indel mutations that result in loss of function (LOF). However, for this system to mutate genes *in vivo*, the RNP complex must be able to form. Adeno-associated viruses (AAV) are an efficient means of transducing cells to deliver plasmid DNA. Swiech et al. demonstrated that AAVs could be used to deliver CRISPR/Cas9 machinery to target genes in the

brain (Swiech et al., 2015). A dual vector system was created where the SpCas9 and the sgRNA were expressed from separate vectors. Co-transduction efficiency of the two viral vectors in mouse primary cortical neurons reached 75% *in vitro*. To test the efficiency of the dual vector system *in vivo*, AAV-SpCas9 and AAV-SpMecp2-GFP-KASH (containing the sgRNA targeting the gene *Mecp2*) were co-injected into the dentate gyrus (DG) of mice. FACS sorting of GFP+ cells from the DG revealed 68% of targeted cells contained mutations in *Mecp2* two weeks post-surgery. *Mecp2* is ubiquitously expressed throughout the brain, and loss of *Mecp2* results in alterations in neuron morphology as well as learning deficits (Chen et al., 2001; Zhou et al., 2006). Cultured neurons expressing both SpCas9 and the sgRNA against *Mecp2* exhibited differences in their dendritic tree morphology and spines. Mice with AAV-SpCas9 and AAV-SpMecp2-GFP-KASH co-injected into the dentate gyrus showed significantly less freezing to a context that they had previously been shocked in, suggesting deficits in contextual memory. This study demonstrated that AAV-mediated CRISPR/Cas9 mutagenesis is robust enough to produce changes in neuron physiology and alter mouse behavioral phenotypes.

Cre-dependent transgenic mouse and rat lines that allow for cell-type specific expression of SpCas9 have also been generated and require the use of only a single viral vector (Back et al., 2019; Platt et al., 2014). Additionally, a Cre-dependent SpCas9 mouse line was created by inserting the gene encoding SpCas9 into the *Rosa26* locus preceded by a floxed sequence that inhibits protein translation without the expression of Cre (Platt et al., 2014). Injection of an AAV carrying an sgRNA targeting *NeuN* into the prefrontal cortex resulted in an indel rate of 85% from FACS sorted GFP+ nuclei.

However, this method requires crossing the SpCas9 conditional lines to Cre-driver lines that can reduce the speed of genetic analysis.

While SpCas9 has been shown to be extremely effective, its large size (4.2kb) limits its use in some biological applications. Ran et al. screened Cas9 endonucleases from six different bacteria that contained a truncated REC domain and therefore were almost 1kb smaller than the canonical SpCas9 (Ran et al., 2015). Similar to SpCas9, they found all six orthologues cleaved double strand DNA 3 bases upstream of PAM. However, only *Staphylococcus aureus* Cas9 (SaCas9) edited DNA with frequencies similar to SpCas9. Using SaCas9, the entire CRISPR/SaCas9 system can be packaged into a single AAV. This further simplifies the system, providing SaCas9 an advantage over SpCas9 in the AAV-CRISPR gene mutagenesis field.

AAV-CRISPR/SaCas9

With only 17% sequence homology, the structure of SaCas9 is remarkably similar to SpCas9 (Nishimasu et al., 2015; Nishimasu et al., 2014). Likewise, SaCas9 can also be divided into a REC lobe and NUC lobe consisting of a WED domain, PI domain, and HNH and RuvC nucleases. While SpCas9 recognizes the PAM sequence 5'NGG3' and uses a17-20bp sgRNA, SaCas9 recognizes 5'NNGRRRT3' and requires a minimum 21bp sgRNA (Ran et al., 2015). Studies using a fluorescence mutagenesis assay directly comparing the cleavage frequencies of SpCas9 vs. SaCas9 found higher activity from SaCas9, suggesting the slightly longer sgRNA and PAM sequence could increase the specificity and efficiency of SaCas9 compared to SpCas9 (Xie et al., 2018).

Using a single AAV containing a Cre-dependent SaCas9 and an sgRNA, it was recently demonstrated that SaCas9 is capable of mediating cell-type specific mutagenesis (Kumar et al., 2018). Surprisingly, the reported efficiency of using this strategy was exceptionally low. Whether this low efficiency was the result of targeting an alternatively spliced exon, the method of analysis to assess mutagenesis, or the inefficiency of the CRISPR/SaCas9 is still unclear. It is also unclear whether viral-based delivery of SaCas9 and the sgRNA from a single AAV can be used in different cell types, or whether other recombinases can be used to provide conditional expression of SaCas9 for gene mutagenesis. To address these questions, we generated a single AAV containing a recombinase-dependent expression cassette for SaCas9 with a non-conditional sgRNA (AAV1-CMV-FLEX-SaCas9-U6-sgRNA). Using a straightforward design for targeting the most 5' conserved exon for a gene of interest, we found this approach to be as efficient as conventional gene knockout. We further demonstrated this approach could be used to target genes in cells that would be otherwise difficult to genetically isolate. Finally, we illustrate that this strategy can be effectively used with either Cre recombinase or Flp recombinase, further expanding our capacity to probe questions requiring manipulation of multiple genes in different cell types.

CHAPTER 2: SINGLE VECTOR CRISPR/SACAS9 IS AS EFFICIENT AS CONVENTIONAL KNOCKOUT

Introduction: design of sgRNAs

To determine the efficiency of a Cre-dependent CRISPR/SaCas9 viral-based system, we first sought to establish a systematic method for the design of sgRNAs. We reasoned that targeting the most 5' common exon of each gene would provide the most reliable inactivation. This is achieved by aligning the genomic sequence obtained from the UCSC Genome Browser (Kent et al., 2002) with reference sequences for all known splice variants from Mouse Genomics Informatics (Bult et al., 2019) (**Figure 1C**). The sequence for the designated exon is analyzed using the CRISPOR prediction tool (crispor.tefor.net) (Concordet and Haeussler, 2018; Haeussler et al., 2016) to identify guides with the highest predicted efficiency and fewest predicted off-targets. Guides are synthesized and subcloned into the AAV shuttle plasmid as described (Ran et al., 2015).

Design of CRISPR/Cas9 constructs

The AAV1 serotype virus is produced in house (Gore et al., 2013). The optimal size of the insert between the ITRs of AAV is 4.7kb, which is the approximate size of the AAV genome (Grieger and Samulski, 2005; Lusby et al., 1980; Muzyczka et al., 1984; Wu et al., 2010). We generated an AAV plasmid containing an inverted SaCas9 flanked by two sets of loxP sites for Cre-mediated inversion and excision (FLEX or DIO), in addition to a U6 promoter and sgRNA (AAV1-CMV-FLEX-SaCas9-U6-sgRNA**, Figure**

1A). With the addition of two sets of loxP sites (to permit stable inversion of SaCas9) the overall size between the ITRs is 4.85kb, which is slightly beyond the optimal AAV insert size. To determine whether reducing the size of the insert would impact conditional mutagenesis, we created a second construct containing only one set of inverted loxP sites (AAV1-CMV-FLEX(1loxP)-SaCas9-U6-sgRNA, **Figure 1B**) that reduced the size to 4.7kb. The disadvantage of this strategy is repeated Cre-mediated inversion that results in constitutive on/off/on/off expression of the transgene that may reduce efficiency.

Initial validation targeting Th and Rosa26

To assess mutagenesis capabilities of AAV1-CMV-FLEX-SaCas9-U6-sgRNA vs. AAV1-CMV-FLEX(1loxP)-SaCas9-U6-sgRNA *in vivo*, we generated AAVs containing a guide targeted to the *Th* allele (**Figure 2A**), which encodes the rate-limiting enzyme in catecholamine production, tyrosine hydroxylase (TH). Co-injection with an AAV expressing EGFP fused to the N-terminus of the KASH domain (AAV1-FLEX-EGFP-KASH) permitted labeling of virally transduced cells and facilitated genomic DNA isolation via FACS for targeted sequencing (**Figure 2A**) (Swiech et al., 2015).

To control for the activation of downstream processes that may alter neuron viability by Cas9-mediated double strand breaks, we generated a guide targeting the *Rosa26* (sgRosa26), a locus that does not have any known function but is highly expressed *in vivo* and used consistently to express exogenous proteins in transgenic mice (Hasegawa et al., 2013; Platt et al., 2014; Soriano, 1999; Srinivas et al., 2001). AAV1-CMV-FLEX-SaCas9-U6-sgTh, AAV1-CMV-FLEX(1loxP)-SaCas9-U6-sgTh, or AAV1-CMV-FLEX-SaCas9-U6-sgRosa26 (control) with AAV1-FLEX-EGFP-KASH was

injected into the VTA of mice expressing Cre recombinase under the control of the endogenous dopamine transporter (DAT) locus *Slc6a3* (DAT-Cre**, Figure 2A**) (Zhuang et al., 2005). Viral targeting resulted in high efficiency transduction that was specific to TH-positive neurons (**Figure 3**). Four weeks after injection, we assessed genetic loss of function through *Th* mutagenesis with viral CRISPR/SaCas9 and compared to *Th* inactivation using a $Th^{lox/lox}$ mouse line (Darvas and Palmiter, 2010) injected with AAV1-CMV-Cre-GFP. Using immunohistochemistry (IHC) with an antibody specific to TH, we determined that both AAV1-CMV-FLEX-SaCas9-U6-sgTh and AAV1-CMV-FLEX(1loxP)-SaCas9-U6-sgTh were as effective at *Th* inactivation as conventional gene knockout (**Figure 2B-E**). Thus, for further CRISPR/SaCas9 mutegenesis experiments, we used the construct containing double lox sites (AAV1-CMV-FLEX-SaCas9-U6-sgRNA).

We also tested if we could achieve loss of TH when using a different sgRNA but targeting the same exon (sgTh2, **Figure 4A-B**) or when using a dual vector non-Cre dependent SpCas9 system targeting *Th* (**Figure 4C-D**). Both of these methods also resulted in a robust knockout of TH (**Figure 4E-F**).

Sequence verification of mutagenesis

FACS facilitated by nuclear envelope-localized EGFP-KASH (AAV1-FLEX-EGFP-KASH) allowed for isolation of targeted and non-targeted cells (**Figure 5**). SaCas9 produces double strand DNA breaks 3 bases upstream of the PAM within the proto-spacer (sgRNA targeted) DNA sequence (Ran et al., 2015). To assess mutagenesis, we isolated nuclei from mice co-injected with AAV1-FLEX-EGFP-KASH

and either AAV1-CMV-FLEX-SaCas9-U6-sgTh or AAV1-CMV-FLEX-SaCas9-U6-sgRosa26, sorted GFP+ nuclei, and then performed whole genome amplification (WGA) on lysed nuclei to uniformly increase the amount of collected genomic DNA for downstream analysis (Deleye et al., 2017). Using WGA DNA, we amplified a~400bp DNA fragment surrounding the intended target within the *Th* and *Rosa26* locus from GFP+ and GFP- nuclei in CRSPR/SaCas9 targeted mice. Sanger sequencing revealed multiple peaks in the chromatogram just upstream of the PAM sequence in both sgRosa26 and sgTh groups (**Figure 5A-B**), consistent with a SaCas9-mediated LOF. Targeted deep sequencing of the amplicons indicated the presence of both deletions and insertions (**Figure 5C-D**). Sequencing of *Th* resulted in 54% of total reads containing mutations, while sequencing of Rosa26 resulted in 38% containing mutations.

Given that our IHC experiments resulted in ~90% loss of TH, we expected the percent of reads with mutations to be much higher than observed. We reasoned this inconsistency between the IHC results and sequencing could be due to auto-fluorescing cells appearing in the Alexa-488 channel during FACS, effectively incorporating GFP- nuclei into the GFP+ group. Thus, restricting nuclei collection to only the brightest GFP+ nuclei would result in a higher mutation frequency.

To test this, we sorted GFP+ nuclei from mice co-injected with AAV1-FLEX-EGFP-KASH and AAV1-CMV-FLEX-SaCas9-U6-sgTh or AAV1-CMV-FLEX-SaCas9-U6-sgRosa26 into either a dim GFP+ gate, bright GFP+ gate, or combined gate (**Figure 6A**). We then performed WGA, PCR, and targeted deep sequencing for both sgRosa26 and sgTh for all three gates (**Figure 6B-C**). As predicted, the amplicons from the

brightest GFP+ gate resulted in ~90% mutagenesis at the target location for both sgRosa26 and sgTh (**Figure 6D-E**).

We contemplated whether to use the combined gate or bright GFP+ gate to confirm mutagenesis for future experiments. While limiting the sort to only the brightest GFP+ nuclei appears to be the most attractive option, there are potential confounds to this approach. For example, the degree of autofluorescence present during FACS can vary from sort to sort by slight variations in viral injection sites, tissue punches taken for nuclei extraction, or by cell types sorted. The red nucleus, located directly dorsal to the VTA, is highly autofluorescent and almost impossible to avoid during VTA nuclei extraction. Tissue punches containing more nuclei from the red nucleus will have greater autofluorescence, contaminating the true GFP+ population in the collection gate. Conversely, it would be difficult to discern nuclei populations with less auto-fluorescence from populations with reduced GFP+, thereby potentially missing mutations with strict gating. Although lowering the percent of mutations overall, using the combined gate will ultimately increase the likelihood of obtaining a complete library of mutations for each sgRNA. For this reason, we used the combined gate to sort GFP+ nuclei for mutagenic analysis in the remaining experiments.

Whole exome sequencing

We performed whole exome sequencing (WES) on WGA DNA extracted from GFP+ and GFP- nuclei from mice co-injected with AAV1-FLEX-EGFP-KASH and AAV1-CMV-FLEX-SaCas9-U6-sgTh or AAV1-CMV-FLEX-SaCas9-U6-sgRosa26 as an unbiased test of whether our single vector system produced off-target mutagenesis

(**Figure 7**). WES revealed 763 insertions or deletions for all four samples combined in exons of 322 genes following correction for known population level mutations. Of the 322 genes, 175 were unique to a single sample and we confirmed insertions or deletions in exons using the Integrative Genomics Viewer (software.broadinstitute.org/software/igv/) (Robinson et al., 2011) in 158 of these. These unique indels were distributed across all four samples (*Rosa26* GFP-positive, 16; *Rosa26* GFP-negative, 86; *Th* GFP-positive, 44; *Th* GFP-negative, 11). The guide directed towards *Gt(Rosa26)Sor* was in intron 1 and not identified by WES. However, this method did confirm indels in exon 2 of the *Th* locus that was located at the site of the SaCas9 cleavage within the sgRNA that was unique to GFP-positive nuclei from mice injected with AAV1-CMV-FLEX-SaCas9-U6-sgTh and AAV1-FLEX-EGFP-KASH.

Figures1-7

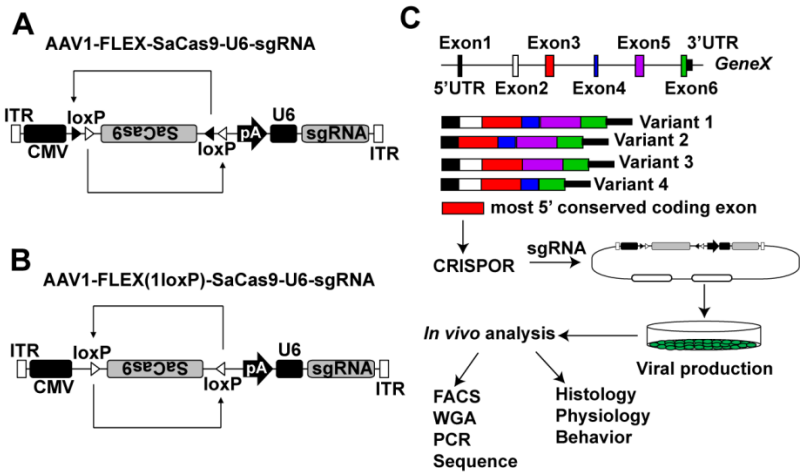

Figure 1: Design of the single vector system
(A) Design of AAV1-FLEX-SaCas9-U6-sgRNA. (B) Design of AAV1-FLEX(1LoxP)-SaCas9-U6-sgRNA. (C) Schematic of the process for designing, generating and analyzing CRISPR/SaCas9 AAVs.

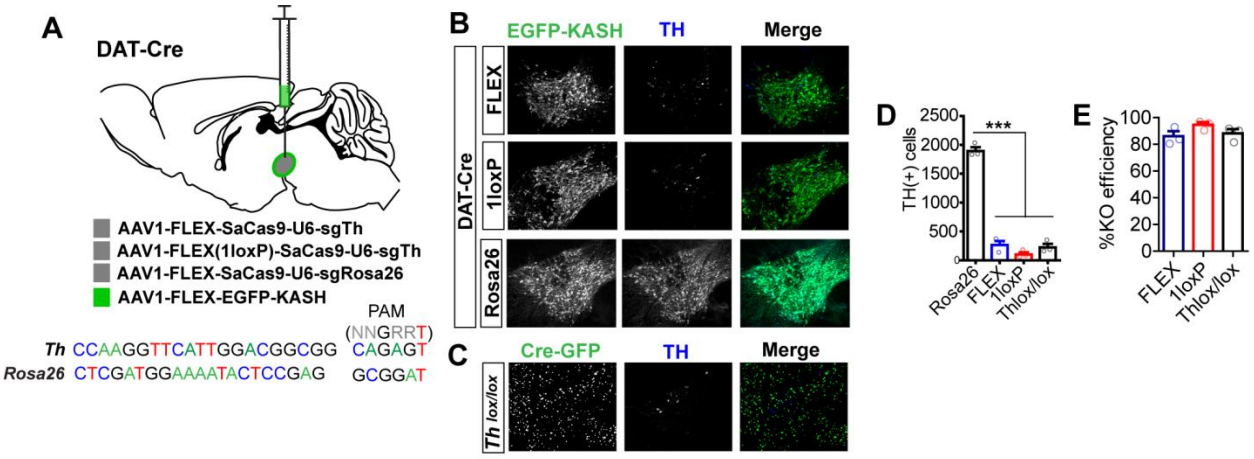

Figure 2: AAV-CRISPR results in robust targeting of *Th*
(A) Illustration of sagittal section showing viral injections into the VTA. (B) Example images of coronal VTA sections co-stained for EGFP (for identifying virally transduced and Cre-positive neurons using AAV1-FLEX-EGFP-KASH) and tyrosine hydroxylase (TH; a marker for dopamine neurons) showing loss of TH staining in the 1loxP and FLEX strategies compared to sgRosa26 controls. (C) Example images of coronal VTA sections co-stained for GFP and TH in $TH^{lox/lox}$ mice injected with AAV1-Cre-GFP. (D) Cell count quantification of VTA TH-positive cells (n=3 mice/group; One-way ANOVA $F_{(3,8)}$=203 P<0.0001; Tukey's multiple comparisons test, ***P<0.001). (E) Comparison of knockout efficiencies between the FLEX-sgTh, 1LoxP-sgTh, and $TH^{lox/lox}$ strategies.

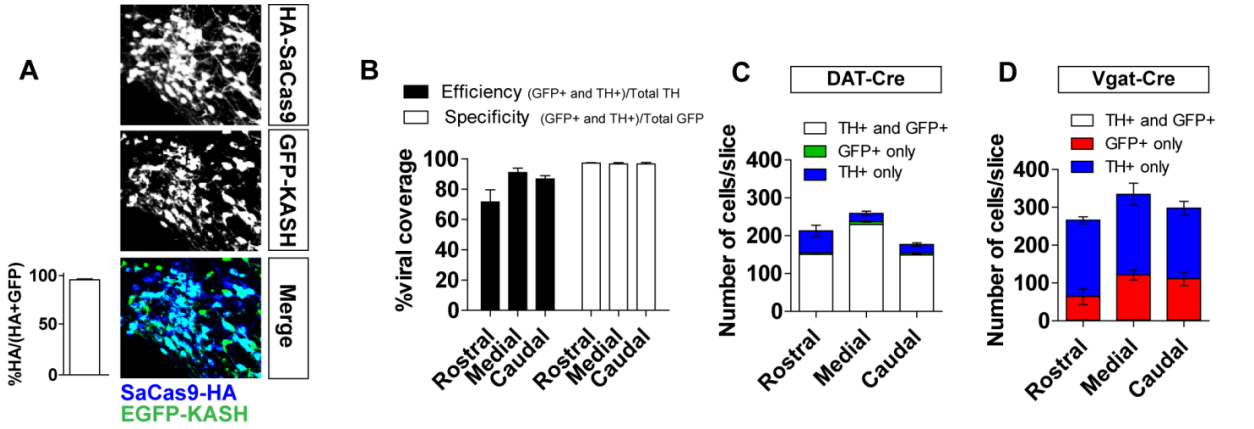

Figure 3: Efficiency and specificity of CRISPR/SaCas9
(A) Example IHC images showing overlap of HA (SaCas9 is fused with an HA tag on the C-terminus) and GFP (AAV1-FLEX-EGFP-KASH). Graph shows overlap of HA and EGFP-KASH. (B) Efficiency and specificity of AAV1-FLEX-SaCas9-U6-sgTh calculated by cell counting TH-positive and GFP-positive cells in mice co-injected with AAV1-FLEX-SaCas9-U6-sgTh and AAV1-DIO-EGFP-KASH (n=3 mice). (C-D) Cell counts in (C) DAT-Cre or (D) Vgat-Cre mice were performed in mice injected with AAV1-FLEX-EGFP-KASH in rostral, medial, and caudal VTA sections (n=3 mice, 3 sections/VTA region). Cell counts were performed using viral labeling with EGFP-KASH as it was a more reliable marker than HA with IHC.

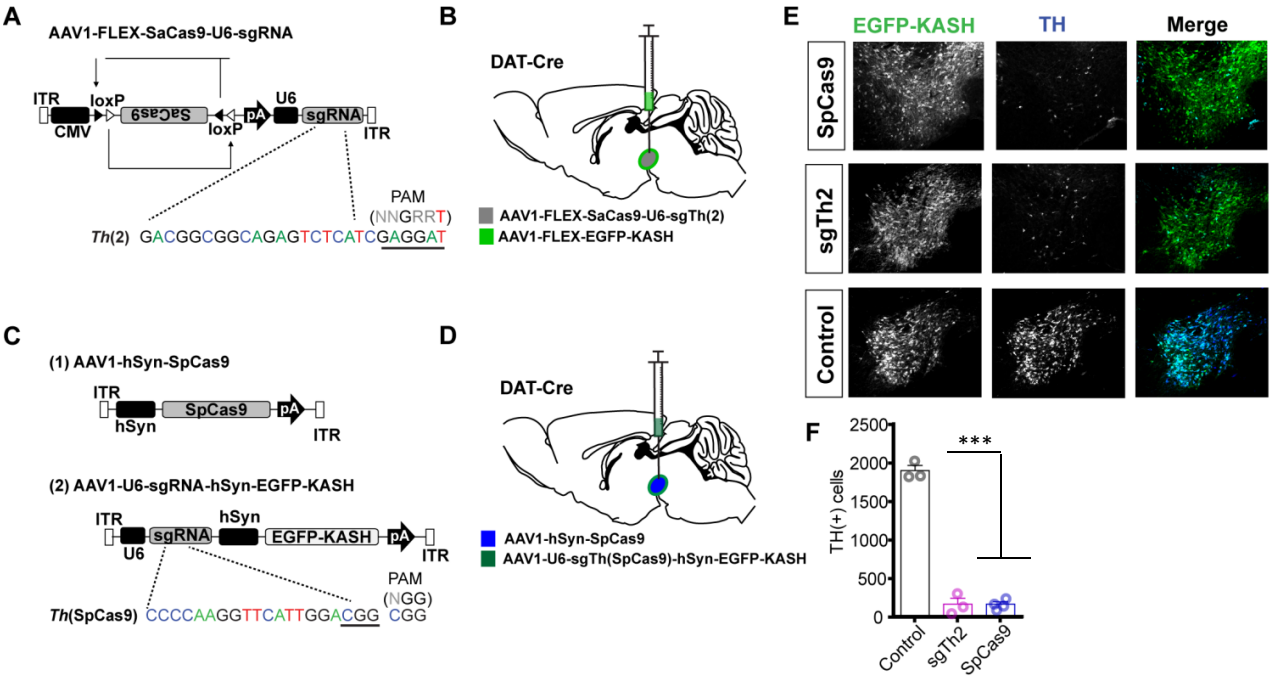

Figure 4: Comparison to sgTh2 and sgTh(SpCas9)
(A) Design of AAV1-FLEX-SaCas9-U6-sgTh(2). (B) Illustration of sagittal section with viral injections into the VTA. (C) Design of AAV1-hSyn-SpCas9 and AAV1-U6-sgTh(SpCas9)-hSyn-EGFP-KASH. (D) Illustration of sagittal section with viral injections into the VTA. (E) Example images of coronal VTA sections co-stained for EGFP (for identifying virally transduced and Cre-positive neurons using AAV1-FLEX-EGFP-KASH) and tyrosine hydroxylase (TH; a marker for dopamine neurons) showing loss of TH staining in sgTh(2) and sgTh(SpCas9) compared to controls. (F) Cell count quantification of VTA TH-positive cells (n=3-4 mice/group; One-way ANOVA $F_{(3,8)}$=203 P<0.0001; Tukey's multiple comparisons test, ***P<0.001).

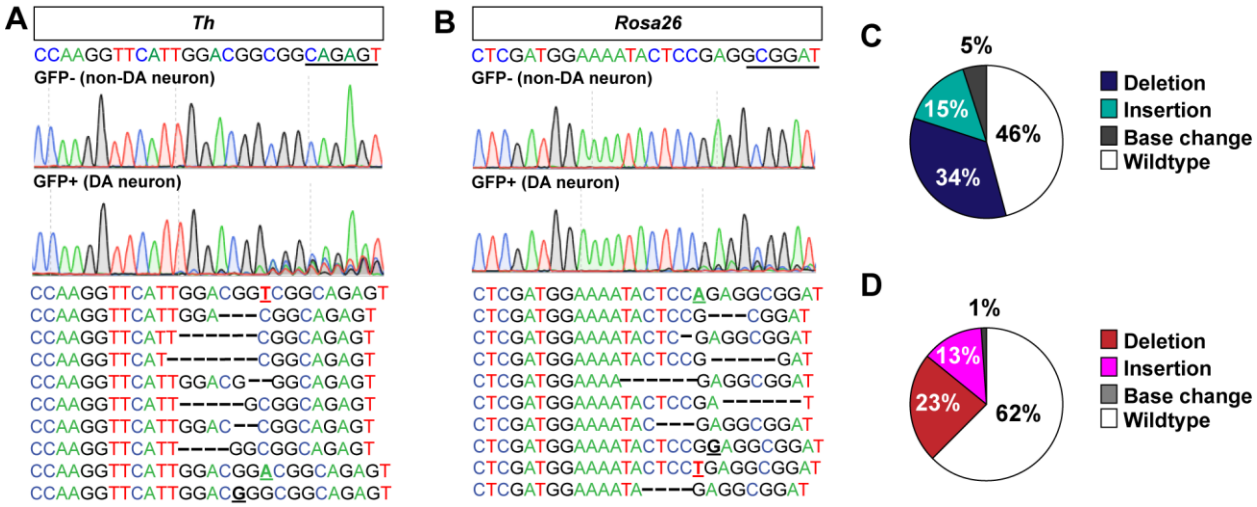

Figure 5: Sequence confirmation of targeting for sgTh and sgRosa26
(A-B) Mice were co-injected with AAV1-FLEX-EGFP-KASH and (A) AAV1-FLEX-SaCas9-sgTh or (B) AAV1-FLEX-SaCas9-sgRosa26. Top: Sanger sequencing of amplicons from sorted GFP+ and GFP- nuclei. Bottom: The top 10 mutations observed in targeted deep sequencing of the GFP+ nuclei. (C-D) Types of mutations observed from targeted deep sequencing of GFP+ nuclei from (C) sgTh or (D) sgRosa26.

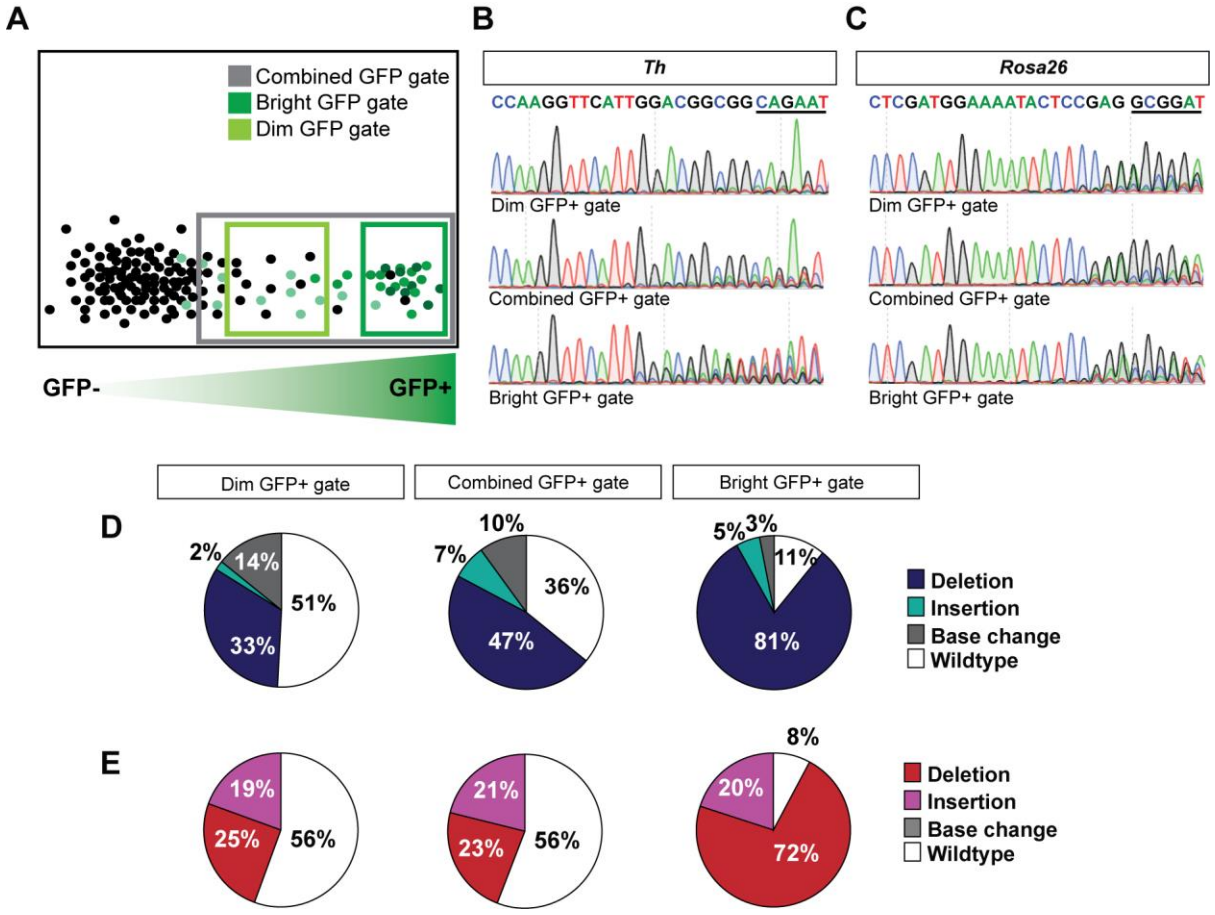

Figure 6: The brightest GFP+ gate has the highest ratio of mutations to wildtype
(A) Diagram of the gates used to collect the GFP+ nuclei from mice co-injected with AAV1-FLEX-EGFP-KASH and AAV1-FLEX-SaCas9-sgTh or AAV1-FLEX-SaCas9-sgRosa26. (B-C) Sanger sequencing of amplicons from GFP+ nuclei collected from the combined, dim, or bright gates for (B) sgTh or (C) sgRosa26. (D-E) Types of mutations observed from targeted deep sequencing of GFP+ nuclei collected from the combined, dim, or bright gates for (D) sgTh or (E) sgRosa26.

GeneName	Sample ID	Indel	GeneName	Sample ID	Indel	GeneName	Sample ID	Indel	GeneName	Sample ID	Indel
4.930467E29R	TH GFP+	deletion	Dab2	Rosa26 GFP +	insertion	Nek3	Rosa26 GFP-	insertion	Tas2r120	Rosa26 GFP-	insertion
Abca13	TH GFP +	insertion	Ddr1	TH GFP +	insertion	Nexmif	Rosa26 GFP-	insertion	Tecta	Th GFP+	insertion
Abl2	TH GFP +	insertion	Dmd	Rosa26 GFP-	insertion	Nexn	TH GFP +	insertion	Trpm7	Rosa26 GFP+	deletion
Acaa2	Rosa26 GFP-	insertion	Dmxl2	Rosa26 GFP +	insertion	Oca2	Rosa26 GFP-	insertion	Tsen15	Rosa26 GFP-	insertion
Adam24	Rosa26 GFP-	insertion	Dok2	TH GFP-	deletion	Olfr1158	Rosa26 GFP-	insertion	Txlnb	Rosa26 GFP-	insertion
Adam24	Rosa26 GFP-	deletion	Enah	Rosa26 GFP-	deletion	Olfr1287	Rosa26 GFP-	insertion	Ube3c	Rosa26 GFP-	insertion
Adam6b	Rosa26 GFP-	insertion	Etl4	TH GFP +	insertion	Olfr1459	Rosa26 GFP+	insertion	Uggt1	Rosa26 GFP-	deletion
Adamts20	TH GFP +	insertion	Fam221a	Rosa26 GFP-	deletion	Olfr389	Rosa26 GFP-	insertion	Usp15	Rosa26 GFP+	insertion
Agap2	TH GFP +	insertion	Gm14744	Rosa26 GFP-	insertion	Olfr574	Rosa26 GFP-	insertion	Usp5	TH GFP +	insertion
Akap6	TH GFP +	insertion	Gm1993	Rosa26 GFP-	insertion	Olfr723	Rosa26 GFP-	insertion	Vmn1r117	Rosa26 GFP-	deletion
Akr1c12	Rosa26 GFP-	insertion	Gm21119	TH GFP-	deletion	Olfr938	Rosa26 GFP-	insertion	Vmn1r31	Rosa26 GFP-	deletion
Aldoa	TH GFP +	insertion	Gm884	Rosa26 GFP-	insertion	Pask	TH GFP-	deletion	Vmn1r61	Rosa26 GFP-	insertion
Anks6	TH GFP +	insertion	Golgb1	Rosa26 GFP-	insertion	Pclo	Rosa26 GFP-	insertion	Vmn2r107	Rosa26 GFP-	insertion
Arcn1	TH GFP -	deletion	Grid2ip	TH GFP +	insertion	Pcm1	Rosa26 GFP-	insertion	Vmn2r116	Rosa26 GFP-	deletion
Ascc1	Rosa26 GFP-	insertion	Grk4	Rosa26 GFP-	insertion	Pcmt1	Rosa26 GFP-	insertion	Vmn2r31	Rosa26 GFP-	insertion
Asxl3	Rosa26 GFP-	insertion	Hal	TH GFP-	deletion	Pcyt1b	Rosa 26 GFP-	deletion	Vmn2r41	Rosa26 GFP-	insertion
Atxn2l	TH GFP +	insertion	Herc1	Rosa26 GFP-	insertion	Pkhd1l1	Rosa 26 GFP-	insertion	Vmn2r78	Rosa26 GFP-	insertion
Avpr1b	TH GFP +	insertion	Hgsnat	Rosa26 GFP-	insertion	Ppp4r4	Rosa 26 GFP-	insertion	Vmn2r90	Rosa26 GFP-	insertion
Axl	TH GFP +	insertion	Hic1	Rosa26 GFP +	insertion	Prrt2	TH GFP+	insertion	Wapl	Rosa26 GFP-	insertion
B3gat3	TH GFP +	insertion	Hnrnpa1l2-ps2	Rosa26 GFP +	deletion	Ptpn14	TH GFP+	insertion	Wdr17	Rosa26 GFP-	insertion
Bcl7c	TH GFP +	insertion	Hsp90ab1	TH GFP-	insertion	Ptpn23	TH GFP+	insertion	Zbtb3	TH GFP +	insertion
Brca2	Rosa26 GFP-	insertion	Ifi44	Rosa26 GFP-	insertion	Rab11fip5	Rosa26 GFP+	insertion	Zcwpw1	Rosa26 GFP-	deletion
Casc3	Rosa26 GFP +	insertion	Igf1r	TH GFP-	insertion	Rabgap1	TH GFP+	insertion	Zfp11	Rosa26 GFP-	deletion
Casp12	Rosa26 GFP-	insertion	Ism2	TH GFP +	insertion	Ranbp2	Rosa26 GFP-	deletion	Zfp362	Rosa 26 GFP+	insertion
Catsperb	Rosa26 GFP-	insertion	Kcnq3	Rosa26 GFP-	insertion	Rbbp6	Rosa26 GFP-	deletion	Zfp446	Rosa 26 GFP+	insertion
Cbr1	TH GFP-	deletion	Kdm5a	Rosa26 GFP +	deletion	Rbbp6	Rosa26 GFP-	deletion	Zfp534	Rosa26 GFP-	insertion
Ccar1	Rosa26 GFP-	insertion	Kif5b	Rosa26 GFP-	insertion	Reg3d	Rosa 26 GFP-	insertion	Zfp583	Rosa26 GFP-	insertion
Ccdc88a	Rosa26 GFP-	insertion	Klhl28	Rosa26 GFP-	insertion	Rfc1	TH GFP+	insertion	Zfp607b	Rosa26 GFP-	insertion
Ccnl1	Rosa26 GFP-	insertion	Kmt2c	TH GFP+	insertion	Rhobtb3	TH GFP-	deletion	Zfp644	Rosa26 GFP-	insertion
Cdc27	Rosa26 GFP +	deletion	Kmt2c	Rosa26 GFP-	insertion	Rhox3f	Rosa 26 GFP-	insertion	Zfp735	Rosa 26 GFP-	insertion
Cdip1	Rosa26 GFP +	insertion	Lrp1b	Rosa26 GFP-	insertion	Rif1	Rosa 26 GFP-	deletion	Zfp735	Rosa 26 GFP-	insertion
Cep112	Rosa26 GFP-	insertion	Lta4h	TH GFP +	insertion	Rnf41	TH GFP+	insertion	Zfpm1	TH GFP +	insertion
Cep126	Rosa26 GFP-	insertion	Map3k11	TH GFP +	insertion	Rp1	Rosa 26 GFP-	insertion	Zhx1	Rosa26 GFP+	insertion
Cep192	Rosa26 GFP-	insertion	Mctp2	Rosa26 GFP-	insertion	Rpf2	Rosa 26 GFP-	insertion	**Th**	**TH GFP+**	**deletion**
Cep55	Rosa26 GFP-	insertion	Mllt6	TH GFP +	insertion	Rtp4	Rosa26 GFP+	insertion	Thrap3	TH GFP-	deletion
Cfap44	Rosa26 GFP-	insertion	Mrgprx1	TH GFP-	insertion	Sall1	TH GFP+	insertion	Tnk2	TH GFP +	insertion
Chd2	TH GFP +	insertion	Mterf1b	Rosa26 GFP-	insertion	Shisa5	TH GFP+	insertion	Tox2	TH GFP +	insertion
Cnksr2	Rosa26 GFP-	deletion	Mtmr11	TH GFP +	insertion	Slc9a6	Rosa26 GFP-	deletion	Trip12	Rosa26 GFP-	insertion
Coq8b	TH GFP+	insertion	Myom1	TH GFP +	insertion	Sos2	Rosa26 GFP-	deletion			
Cthrc1	TH GFP +	insertion	Nabp1	Rosa26 GFP-	insertion	Spen	TH GFP+	insertion			
Ctse	TH GFP +	insertion	Nbea	Rosa26 GFP-	deletion	Sult3a1	Rosa26 GFP-	insertion			

Sample ID	Total Insertions	Total deletions	Insertion/deletion ratio
TH GFP(+)	134	77	1.74
TH GFP(-)	131	54	2.43
Rosa26 GFP(+)	76	65	1.17
Rosa26 GFP(-)	170	56	3.04

Figure 7: Whole exome sequencing
Upper table: WES indel statistics for unique sites after removing known population level indels. Bolded and underlined shows indel in *Th* locus.
Lower table: List of NGS WES indel statistics after removing known population level indels.

CHAPTER 3: CRISPR/SACAS9 CIRCUMVENTS DRAWBACKS OF CONVENTIONAL GENETICS

Introduction

A caveat to conventional Cre-loxP strategies is the observation that many genes can be transiently expressed in germ cells, which can yield mosaic genotypes (Song and Palmiter, 2018). This requires the generation of heterozygous delta (constitutively inactivated) alleles to guard against mosaicism (Song and Palmiter, 2018; Zweifel et al., 2008). A limitation to this strategy is the possibility for haploinsufficiency phenotypes in designated control mice. To establish whether AAV1-CMV-FLEX-SaCas9-U6-sgRNA can be used to circumvent this problem, we targeted the gene encoding the calcium activated, small conductance potassium channel SK3, *Kcnn3* (**Figure 8A**). SK3 is the predominant ion channel underlying SK-mediated tail currents in dopamine neurons (Sarpal et al., 2004; Wolfart et al., 2001), the currents are easy to measure with whole-cell patch clamp using slice electrophysiology, and *Kcnn3* has been conditionally inactivated in dopamine neurons previously using conventional methodologies (Deignan et al., 2012).

Targeting Kcnn3 using sgKcnn3

Because using *Slc6a3* as a Cre-driver can result in ectopic recombination in germ cells, we generated a delta allele for *Kcnn3* by crossing $Kcnn3^{lox/lox}$ mice to a broadly expressed Cre-driver line, Mox2-Cre, as previously described (Zweifel et al., 2008). $Kcnn3^{\Delta}$ mice were crossed to DAT-Cre mice and the resulting DAT-Cre::$Kcnn3^{\Delta/+}$

mice were crossed to *Kcnn3*$^{lox/lox}$ mice to generate wild-type (WT) mice (e.g. *Slc6a3*$^{+/+}$::*Kcnn3*$^{+/lox}$), heterozygous mice (e.g. *Slc6a3*$^{+/+}$::*Kcnn3*$^{\Delta/lox}$ or *Slc6a3*$^{Cre/+}$::*Kcnn3*$^{+/lox}$), and knockout mice (e.g. *Slc6a3*$^{Cre/+}$::*Kcnn3*$^{\Delta/lox}$). Consistent with a haploinsufficiency phenotype, heterozygous mice displayed a reduced SK-mediated tail current in dopamine neurons that was further reduced by biallelic inactivation (**Figure 8D**). Importantly, inactivation of *Kcnn3* using AAV1-CMV-FLEX-SaCas9-U6-sgKcnn3 in the VTA of DAT-Cre mice (**Figure 8B**) was as efficient as conditional gene knockout at reducing SK3-mediated tail currents (**Figure 8C-D**). As described previously, a small SK-mediated current remains in dopamine neurons following *Kcnn3* knockout (Deignan et al., 2012) as demonstrated by an additional reduction in current using the SK-specific toxin apamin (**Figure 8D**) that is likely mediated by SK2 channels. Consistent with previous reports that SK3 channels regulate dopamine neuron activity patterns (Shepard and Bunney, 1991; Soden et al., 2013; Wolfart et al., 2001), *Kcnn3* mutagenesis with AAV1-CMV-FLEX-SaCas9-U6-sgKcnn3 significantly increased spike firing irregularity (**Figure 8E-F**) without altering firing frequency (**Figure 8G**).

Sequence verification of mutagenesis

To determine mutagenesis of *Kcnn3* and the CRISPOR predicted sgKcnn3 off-target in an exon of *Socs6* (Concordet and Haeussler, 2018; Haeussler et al., 2016), GFP+ nuclei were collected from mice co-injected with AAV1-CMV-FLEX-SaCas9-U6-sgKcnn3 and AAV1-FLEX-EGFP-KASH via FACS. Amplicons from WGA DNA from GFP+ nuclei were generated and sent for sequencing. Sanger sequencing of *Kcnn3* revealed the presence of multiple peaks in the chromatogram at the predicted SaCas9

cleavage site, while the sequencing for *Socs6* appeared wildtype (**Figure 9A-B**). Deep sequencing of *Kcnn3* and *Socs6* further confirmed mutagenesis of *Kcnn3* in GFP+ neurons, with 45% of reads containing a deletion mutation. In contrast, *Socs6* displayed 99% wildtype reads, with a less than 1% mutation rate. Thus, viral-mediated CRISPR/SaCas9 is an efficient means to assess ion channel regulation of neural activity and can circumvent issues relating to genetic mosaicism and complex breeding strategies associated with some Cre/loxP genetic approaches.

Figures 8-9

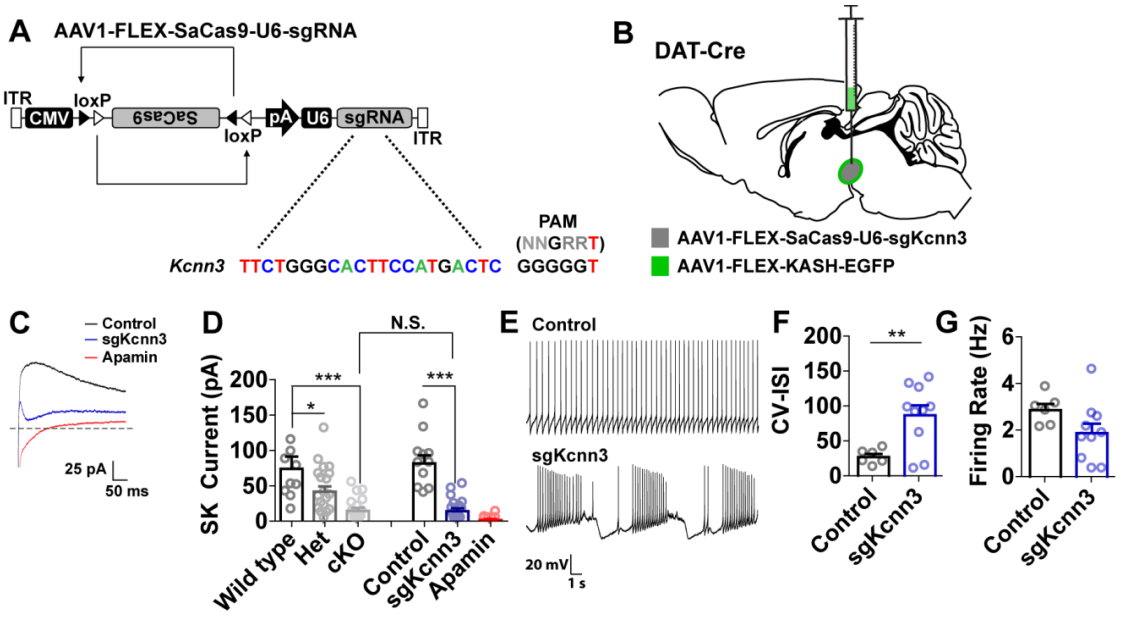

Figure 8: *Kcnn3* knockout with viral CRISPR/Cas9 is as efficient as Cre/loxP-mediated knockout
(A) Design of AAV1-FLEX-SaCas9-U6-sgKcnn3. (B) Illustration of sagittal section with viral injections into the VTA. (C) Example traces of tail currents in dopamine neurons evoked following a 500 ms step from -70 to 0 mV. (D) Quantification of tail current amplitudes following genetic knockout or sgKcnn3, or application of apamin (Wild type n=10, Het n=19, cKO n=15, Control n=11, sgKcnn3 n=15, apamin n=6; One way ANOVA $F_{(5, 70)}$=12.05 P<0.0001; Bonferroni's Select Comparison *P<0.05, ***P<0.001). (E) Example traces of action potential firing recorded in slice from control or sgKcnn3-expressing dopamine neurons. (F-G) Quantification of the (F) coefficient of variation of the inter-spike interval and (G) firing rate in control or sgKcnn3-expressing dopamine neurons recorded in slice (Control n=6, sgKcnn3 n=19; Student's t test **P<0.01).

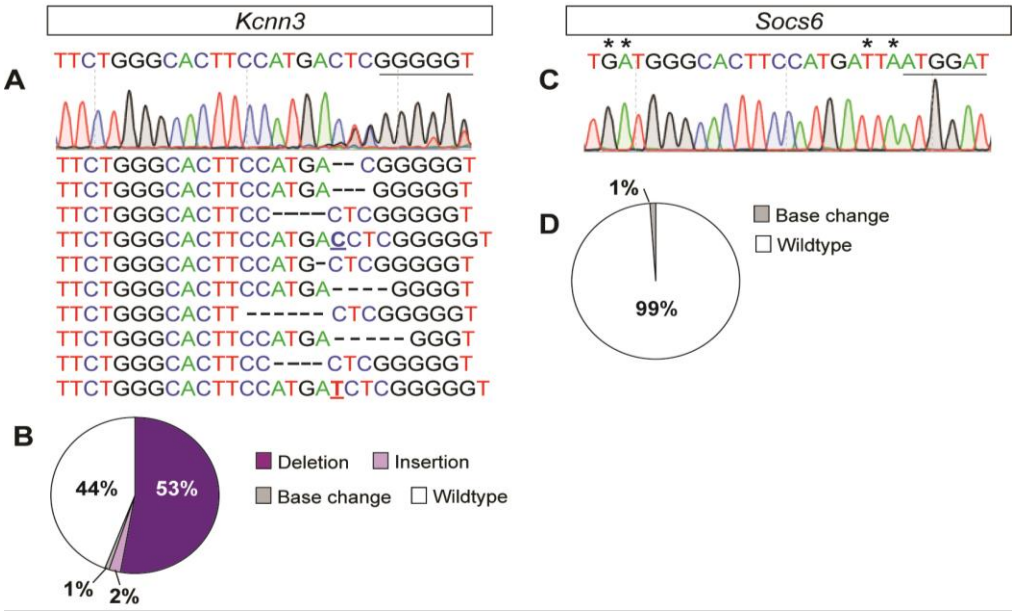

Figure 9: Sequencing confirmation of sgKcnn3 targeting

(A) Sanger sequencing of PCR amplicons for *Kcnn3* from FACS sorted GFP-positive nuclei from the combined gate of mice co-injected with AAV1-FLEX-SaCas9-U6-sgKcnn3 and AAV1-FLEX-EGFP-KASH into the VTA of DAT-Cre mice, and the most common indels in *Kcnn3* (bottom). (B) Percentage of sequence reads with wild-type, insertion, deletion, or base changes for *Kcnn3*. (C) Sanger sequencing of PCR amplicons for *Socs6,* asterisks denote base mismatches relative to *Kcnn3* guide. (D) Percentage of sequence reads with wild-type, insertion, deletion, or base changes for *Socs6*.

CHAPTER 4: CRISPR/SACAS9 CAN TARGET UBIQUITOUSLY EXPRESSED GENES IN DIFFICULT TO ISOLATE CELL TYPES

Introduction

The VTA consists of multiple cell types including GABAergic, dopaminergic, and glutamatergic populations (Lammel et al., 2014; Morales and Margolis, 2017). Because of their restricted distribution to a small number of regions in the brain, Cre-driver lines such as DAT-Cre can provide a relatively selective means for the study of gene function using conventional gene inactivation strategies. In contrast, populations such as VTA GABA-producing cells that do not have identifiable markers that allow for both neurotransmitter and anatomical specificity are more difficult to isolate for selective gene inactivation experiments.

To assess the efficiency of mutagenesis in cells that have been previously difficult to manipulate genetically, we targeted a broadly expressed gene that plays a key role in GABAergic synaptic transmission, *Gabrg2*, which encodes the $GABA_A$ receptor subunit $\gamma 2$. Within the VTA, both dopaminergic and GABAergic neurons express $GABA_A$ receptors. The $GABA_A$ γ2 subunit is required for proper $GABA_A$ receptor formation and insertion into the cell membrane at the synapse (Schweizer et al., 2003). To selectively mutate *Gabrg2*, we generated AAV1-CMV-FLEX-SaCas9-U6-sgGabrg2 (**Figure 10A**) for selective mutagenesis in either GABA neurons (Vgat-Cre) or dopamine neurons (DAT-Cre) (**Figure 10B**). Viral labeling of GABA producing neurons in the VTA did not overlap with TH in the VTA, indicating specificity for viral transduction (**Figure 3D**).

Design of controls

In addition to addressing the role of $GABA_A$ receptor signaling in GABAergic neurons of the VTA, we sought to establish a broadly useful strategy for controlling AAV1-CMV-FLEX-SaCas9-U6-sgRNA expression. It has been shown that the bases within the seed region of the sgRNA directly adjacent to the PAM site are crucial for the unwinding of DNA and subsequent mutagenesis by SaCas9 (Jiang et al., 2015; Nishiyama et al., 2017; Sternberg et al., 2014). Therefore as a negative control, we generated an identical guide for targeting *Gabrg2* but mutated three bases in the seed region (sg*Gabrg2TTT,* **Figure 10A**).

Sequence verification of mutagenesis

To test whether the control sgRNA prevents mutagenesis of *Gabrg2*, we co-injected mice with AAV1-FLEX-EGFP-KASH and either AAV1-CMV-FLEX-SaCas9-U6-sgGabrg2 or AAV1-CMV-FLEX-SaCas9-U6-sgGabrg2TTT and isolated nuclei via FACS. WGA was performed to increase the amount of collected genomic DNA. Sanger sequencing of a PCR-amplified fragment of genomic DNA that included the SaCas9-targeted locus demonstrated a lack of mutagenesis in control (*Gabrg2TTT*) GFP+ nuclei (**Figure 11B**). In contrast, the amplicon from the sgGabrg2 GFP+ nuclei contained multiple nucleotide peaks beginning at the location of the predicted cut site, signifying *Gabrg2* gene mutagenesis (**Figure 11A**). Targeted deep sequencing of the amplicon further confirmed mutagenesis only in experimental mice (**Figure 11D-E**). In addition to sequencing across the predicted SaCas9 targeting site, we also sequenced amplicons containing CRISPOR predicted off-target sites within an exon (Figure 11C) (Concordet

and Haeussler, 2018; Haeussler et al., 2016). While Sanger sequencing exhibited only wildtype sequences, deep sequencing of *Paxbp1* and *Wdfy3* off-targets exhibited 88% and 96% wildtype, respectively (**Figure 11F-G**).

Functional verification of sgGabrg2

To quantify the degree of LOF of *Gabrg2* following mutagenesis, we recorded miniature inhibitory postsynaptic currents (mIPSCs) in CRISPR/SaCas9 targeted VTA dopamine and VTA GABA neurons. Mutagenesis of *Gabrg2* in VTA dopamine neurons (**Figure 10C-F**) and in VTA GABA neurons (**Figure 10G-J**) resulted in a significant reduction in mIPSC frequency and amplitude relative to their corresponding controls.

Mutagenesis of Gabrg2 in distinct VTA subtypes bidirectionally alters locomotor activity

The VTA is an important regulator of psychomotor activation and behavioral sensitization of psychostimulant drugs such as cocaine. Although GABAergic signaling plays an important role in these processes (Bocklisch et al., 2013; Cameron and Williams, 1994; Liu et al., 2005; Steffensen et al., 2008) the role of GABAergic signaling in GABA neurons of the VTA is largely unknown. Analysis of basal locomotion revealed that reduced synaptic GABA signaling onto VTA GABA-producing neurons resulted in a significant reduction in distance traveled (**Figure 12**). In contrast, reducing synaptic GABA signaling in dopamine neurons had no significant effect compared to controls (**Figure 12**).

Subcutaneous cocaine injections produce psychomotor activation that increases with subsequent injections (Kalivas and Stewart, 1991). To determine if *Gabrg2*

mutagenesis in VTA GABA and dopamine subpopulations alters psychomotor sensitization, we performed 5 days of repeated cocaine injections (20 mg/kg s.c., once daily, **Figure 13**) and recorded distance traveled pre and post injection. Mutagenesis of *Gabrg2* in VTA GABA producing neurons resulted in a significant attenuation of locomotor sensitization relative to controls or mutagenesis of *Gabrg2* in VTA dopamine producing neurons (**Figure 13**) demonstrating a key role for GABAergic regulation of VTA GABA producing neurons in this process.

Figures 10-13

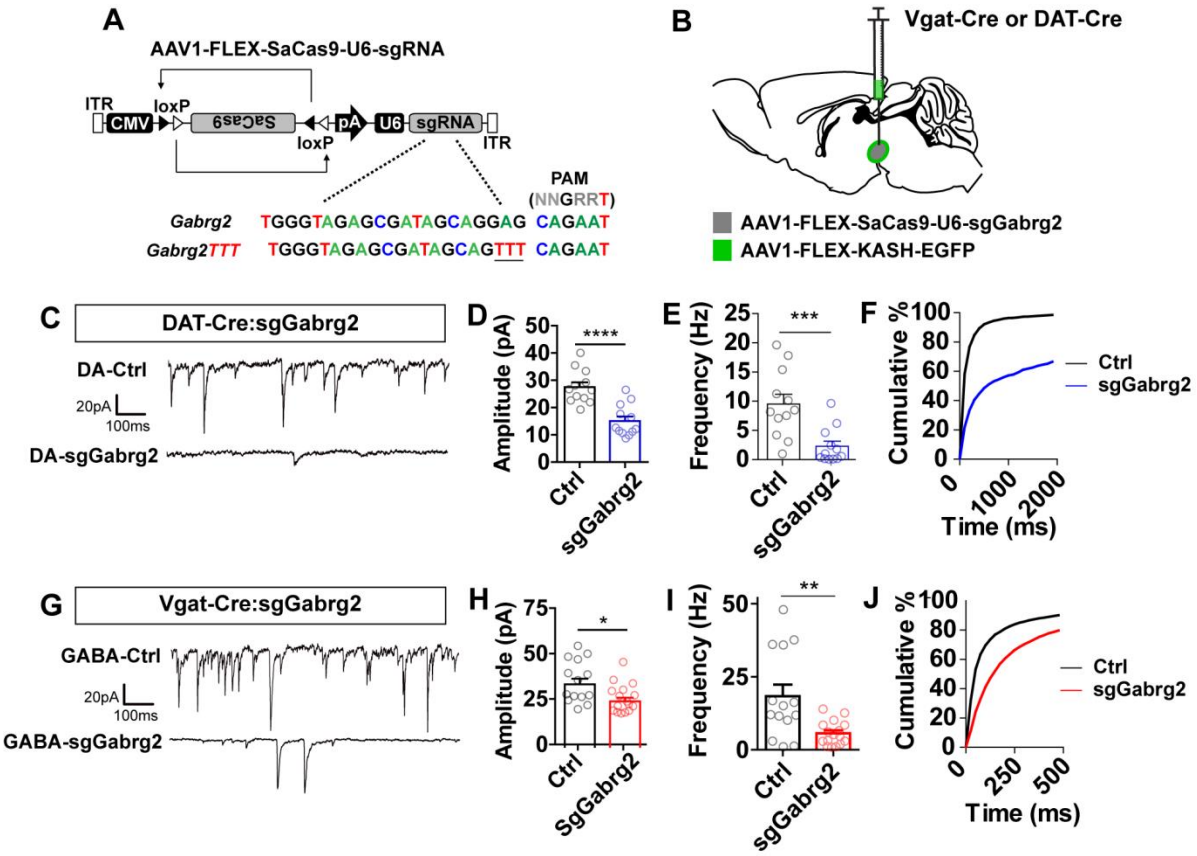

Figure 10: *Gabrg2* knockout with viral CRISPR/Cas9 reduces mIPSCs
(A) Design of AAV1-FLEX-SaCas9-U6-sgGabrg2 and control virus AAV1-FLEX-SaCas9-U6-sgGabrg2TTT. (B) Illustration of sagittal section with viral injections into the VTA. (C-D) Representative traces and quantification of mIPSC amplitude, frequency, and cumulative distribution of inter-event intervals recorded from VTA (C-F) dopamine (n=12 cells/group) or (G-J) GABA (controls n=14 cells, sgGabrg2 n=16 cells) cells. (Student's t test **P<0.01, ***P<0.001).

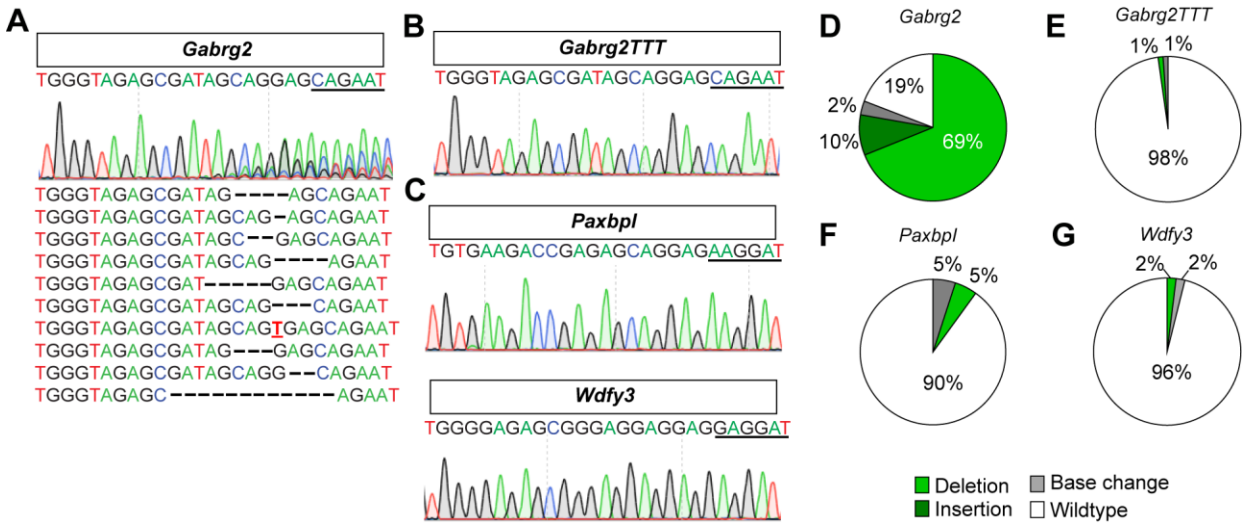

Figure 11: Sequencing confirmation of targeting by sgGabrg2
(A-C) Mice were co-injected with AAV1-FLEX-EGFP-KASH and (A and C) AAV1-FLEX-SaCas9-sgGabrg2 or (B) AAV1-FLEX-SaCas9-sgGabrg2TTT. (A) Targeted Sanger sequencing of *Gabrg2* amplicons from GFP+ nuclei with the top 10 mutations observed in targeted deep sequencing. (B) Targeted Sanger sequencing of *Gabrg2* amplicons from GFP+ nuclei. (C) Targeted Sanger sequencing of CRISPOR predicted off-targets *Paxpbl* and *Wdfy3* from GFP+ nuclei and (D-G) Types of mutations observed from targeted deep sequencing of (D) *Gabrg2*, (E) *Gabrg2* (sgGabrg2TTT mice), (F) *Paxbp1*, and (G) *Wdfy3* amplicons from GFP+ nuclei.

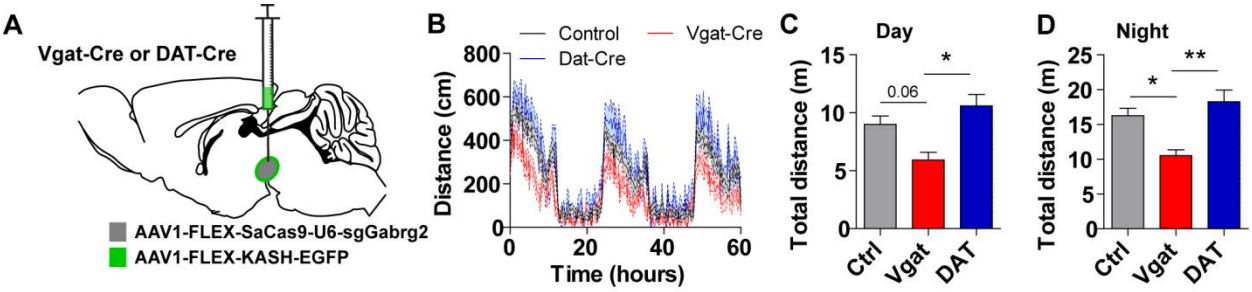

Figure 12: *Gabrg2* mutagenesis in different VTA cell types results in differential behavioral outcomes
(A) Illustration of sagittal section with viral injections into the VTA. (B-D) Comparison of locomotion between Vgat-Cre (n=13) , DAT-Cre (n=13), and control mice (n=44) (B) across three consecutive days and nights in 15 minute time bins, (C) the sum of total distance travelled across two consecutive days (One-way ANOVA $F_{(2,66)}$=4.179, P<0.05; Tukey's multiple comparisons test, *P<0.05) and (D) the sum of total distance travelled across three consecutive nights (One-way ANOVA , $F_{(2,66)}$=5.363, P<0.001; Tukey's multiple comparisons test, *P<0.05, **P<0.01).

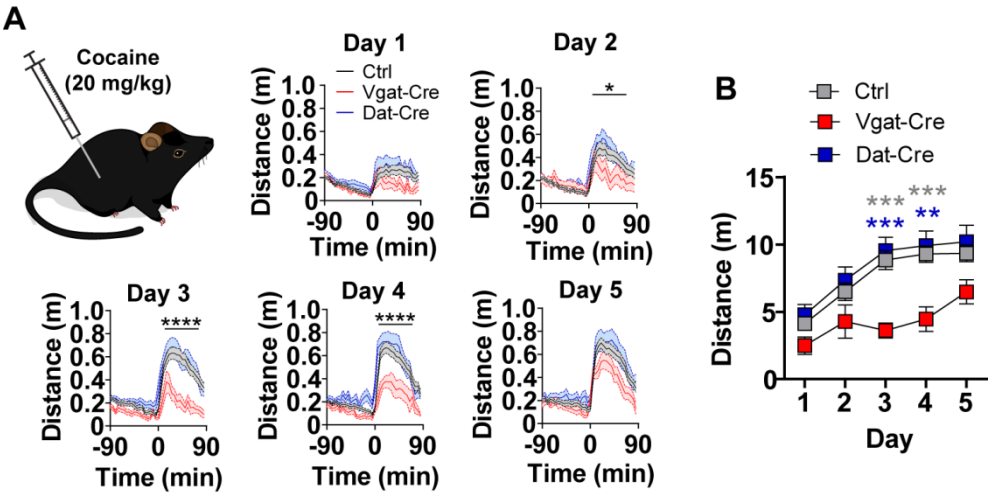

Figure 13: *Gabrg2* mutagenesis in different VTA cell types results in differential behavioral outcomes

(A) Locomotor responses 90 minutes pre and post cocaine (20mg/kg, s.c. injection) injection across five consecutive days in Vgat-Cre, DAT-Cre, and control mice. (B) Sum of 90 minute total distance travelled post cocaine injection for five consecutive days in Vgat-Cre, DAT-Cre, and control mice (Two-way repeated measures ANOVA, effect of genotype, $F_{(2,54)}$=6.259, P<0.01; Tukey's multiple comparisons test, **P<0.01, ***P<0.001).

CHAPTER 5: CRISPR/SACAS9 IS EFFECTIVE FOR PROJECTION-SPECIFIC PHENOTYPIC ANALYSIS

Introduction

Our previous experiments established AAV1-CMV-FLEX-SaCas9-U6-sgRNA can be used to achieve high efficiency gene inactivation through mutagenesis in multiple cell types. We next sought to determine whether this approach can be used for projection-specific phenotypic analysis. It has been previously shown that constitutive global inactivation of the DAT gene, *Slc6a3*, in mice results in robust hyperlocomotor activity (Giros et al., 1996). It has not been established whether this hyperlocomotor phenotype can be observed through the selective adult inactivation of *Slc6a3* in the VTA, more specifically, in the dopamine projection to the nucleus accumbens (NAc).

Verification of loss of DAT

To address this question, we performed parallel experiments in which we injected an AAV1-CMV-FLEX-SaCas9-U6-sgRNA containing a guide targeted to *Slc6a3* (**Figure 14A**) directly into the VTA of DAT-Cre mice (VTA targeted, **Figure 14B**) or injected the retrograde transducing virus CAV containing an expression cassette for Cre (CAV2-CMV-Cre) into the NAc and AAV1-CMV-FLEX-SaCas9-Ug-sgSlc6a3 into the VTA (intersect targeted, **Figure 14C**). Western blot analysis of DAT protein levels from tissue punches of the NAc to isolate dopamine terminals demonstrated significant reductions in both VTA targeted and intersect targeted mice (**Figure 14D-E**). We did not observe significant reductions in TH protein levels in the NAc tissue punches of these mice

(**Figure 15A**), indicating that compensatory downregulation of TH is not observed with this genetic strategy (Salvatore et al., 2016). Reductions in DAT protein in the NAc and VTA were also observed by immunohistochemistry (**Figure 15B**).

Knockout of DAT results in hyperactivity

Analysis of locomotion revealed significant elevations in both day and night distance traveled in VTA targeted and intersect targeted mice (**Figure 16A-F**). In addition to inducing a hyperlocomotor phenotype, congenital inactivation of *Slc6a3* globally is also associated with insensitivity to cocaine (Giros et al., 1996). The contribution of mesolimbic dopamine projections from the VTA to the NAc in mediating this cocaine insensitivity is not known. To address this, we assessed locomotor activity in response to 5 days repeated cocaine injections (20 mg/kg s.c., once daily) in VTA and intersect targeted mice (**Figure 17**). Both intersect and VTA targeted mice showed an initial response to cocaine that did not differ significantly from control mice. With repeated injections, control mice developed a sensitized response as predicted, but VTA and intersect targeted mice displayed a locomotor desensitization that was significantly different from control mice (**Figure 17D**).

Sequence verification of mutagenesis

Genomic DNA from sorted GFP+ nuclei from the VTA of mice injected with AAV1-FLEX-EGFP-KASH and either AAV1-FLEX-SaCas9-sgSlc6a3 or AAV1-FLEX-SaCas9-sgSlc6a3TTT was collected. Following WGA, amplicons were generated that contained sequence surrounding the predicted cut site in *Slc6a3* and its CRISPOR

predicted exon off-target *Ndn*. Sanger and deep sequencing of *Slc6a3* and *Ndn* in the control (sgSlc6a3TTT) and experimental mice, respectively, exhibited almost all wildtype sequences (**Figure 18B and D**). In contrast, Sanger and deep sequencing of *Slc6a3* from experimental mice resulted in gene mutagenesis at the SaCas9 cleavage site (**Figure 18A and C**).

Figures 14-18

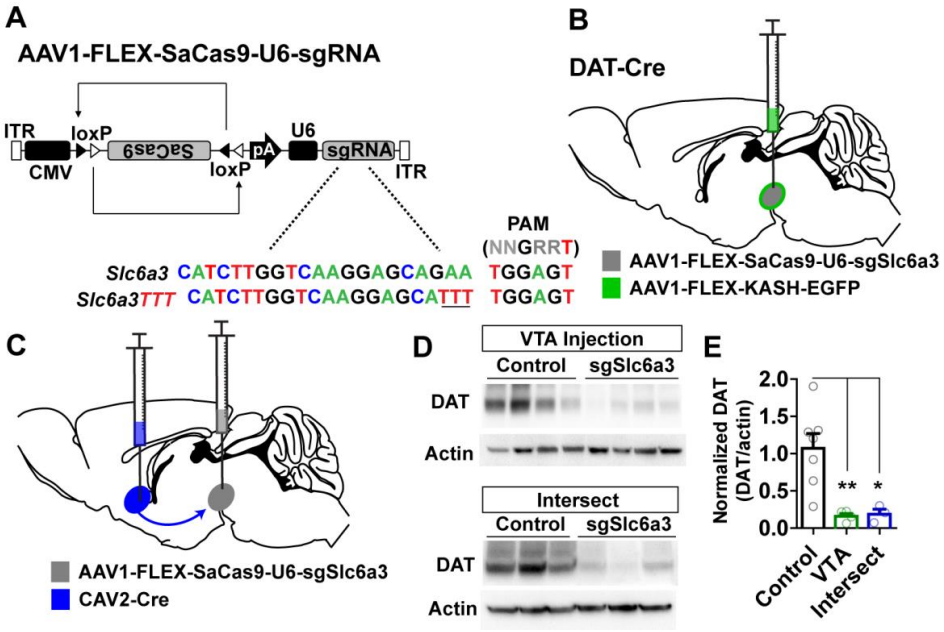

Figure 14: A single injection an intersectional strategy targeting *Slc6a3* produces robust DAT knockout
(A) Design of AAV1-FLEX-SaCas9-U6-sgSlc6a3 and control virus AAV1-FLEX-SaCas9-U6-sgSlc6a3TTT. (B) Illustration of sagittal section with viral injections into the VTA. (C) Illustration of intersectional strategy with injection of CAV2-Cre into the terminals of VTA dopamine neurons in the nucleus accumbens (NAc) and AAV1-FLEX-SaCas9-U6-sgSlc6a3 into VTA dopamine cell bodies in wildtype mice. (D) Western blots from NAc punches probing for DAT and actin comparing the single AAV1-FLEX-SaCas9-U6-sgSlc6a3 VTA injection and the intersect strategy to controls. (E) Quantification of DAT levels from the Western Blots (controls n=7, VTA sgSlc6a3 n=4, VTA-NAc sgSlc6a3 n=3; One-way ANOVA $F_{(2,11)}$=9.055, P<0.001; Tukey's multiple comparisons test *P<0.05, **P<0.01).

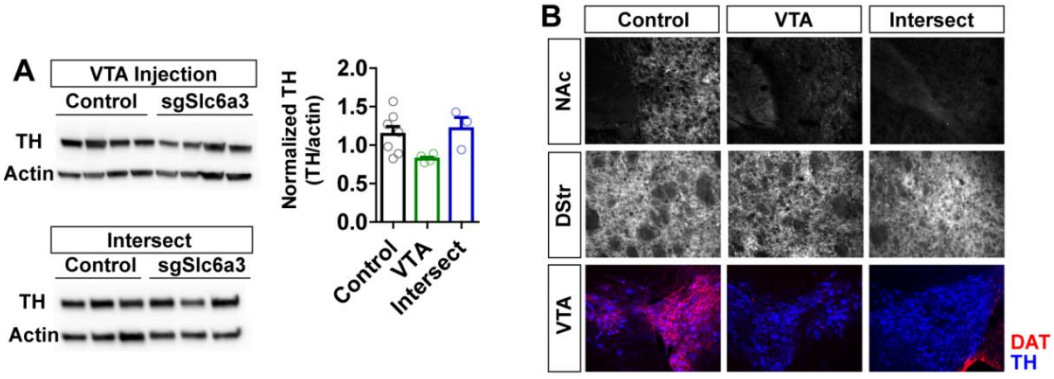

Figure 15: Targeting of *Slc6a3* does not reduce TH levels
(A) Left, top: Western blot probing for TH in control sgSlc6a3TTT mice or sgSlc6a3 injected in the VTA (n=4 mice/group). Left, bottom: Western blot probing for TH in control sgSlc6a3TTT mice or mice injected with CAV2-Cre in the nucleus accumbens (NAc) and AAV1-FLEX-SaCas9-U6-sgSlc6a3 in the VTA (n=3 mice/group). Right: Graph of TH levels normalized to actin shows no significant difference between

controls and sgSlc6a3 targeted mice. (B) Example IHC images of DAT and TH in the NAc, dorsal striatum (DStr) and VTA in control, VTA targeted, or intersect strategy mice.

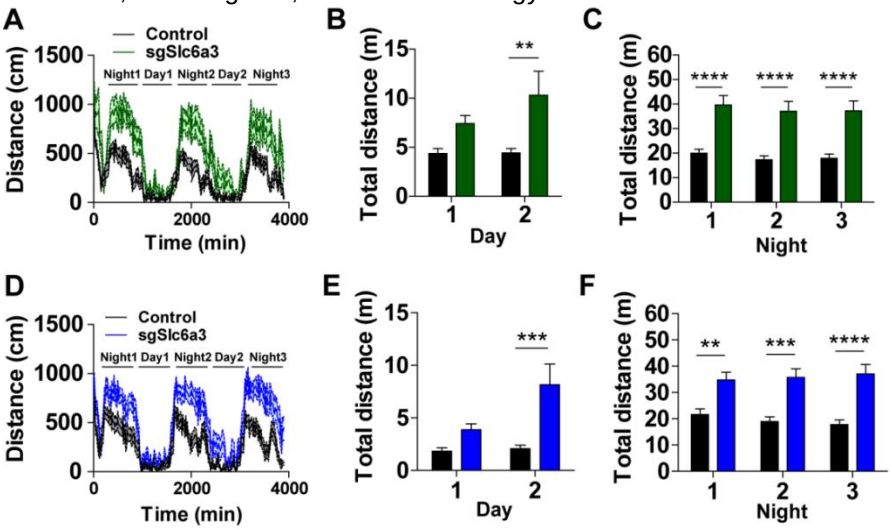

Figure 16: Hyperlocomotion in sgSlc6a3 mice

(A-C) Locomotion measured for the single AAV1-FLEX-SaCas9-U6-sgSlc6a3 VTA injection (controls n=16, sgSlc6a3 n=15), (A) across three consecutive days and nights in 15 minute time bins, (B) comparison of total distance traveled across two consecutive days (Two-way repeated measures ANOVA , effect of virus, $F_{(1,29)}$=8.05, P<0.01; Bonferroni multiple comparisons **P<0.01), and (C) comparison of total distance travelled across three consecutive nights (Two-way repeated measures ANOVA , effect of genotype, $F_{(1,29)}$=23.66 P<0.0001; Bonferroni multiple comparisons ****P<0.0001). (D-F) Locomotion measured for the intersectional strategy, (D) across three consecutive days and nights in 15 minute time bins (controls n=14, sgSlc6a3 n=17), (E) comparison of total distance travelled across two consecutive days (Two-way repeated measures ANOVA , interaction (time x virus), F(1,29)=4.46, P<0.05; Bonferroni multiple comparisons ***P<0.001), and (F) comparison of total distance travelled across three consecutive nights (Two-way repeated measures ANOVA , effect of virus, $F_{(1,29)}$=19.65, P<0.0001, Bonferroni multiple comparisons **P<0.01, ***P<0.001, ****P<0.0001).

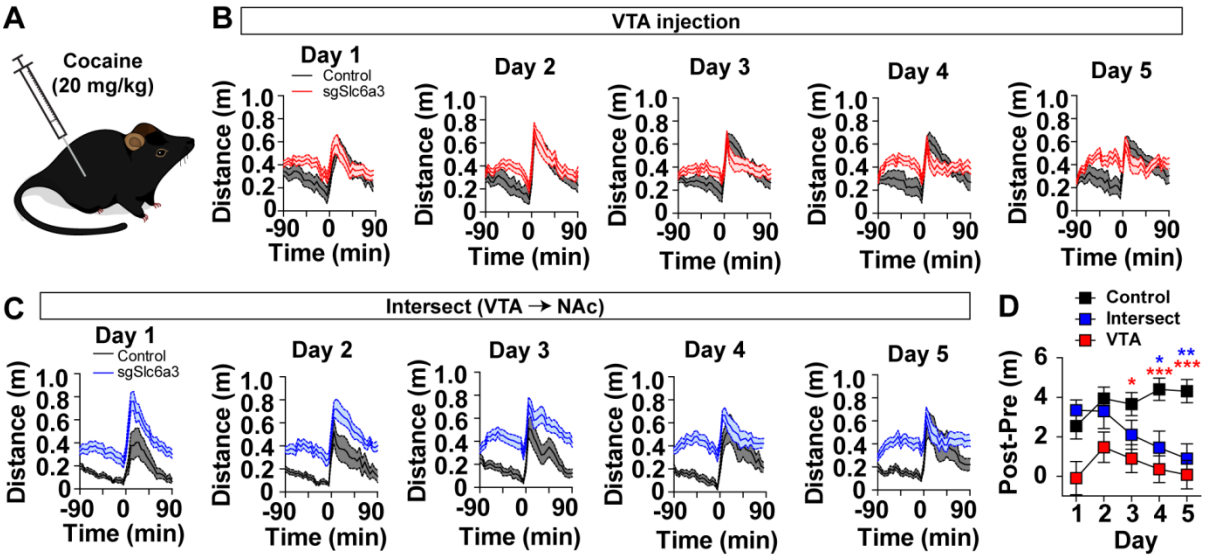

Figure 17: *Slc6a3* targeting by sgSlc6a3 produces insensitivity to repeated cocaine

(A) Cartoon of s.c. cocaine injection for locomotor sensitization. (B-D) Locomotor responses 90 minutes pre and post cocaine (20mg/kg) injection across five consecutive days in (B) VTA targeted or (C) intersect strategy mice. (D) Sum of the pre cocaine injection distance traveled substracted from the post cocaine

injection distance for five consecutive days in VTA targeted or intersect strategy mice (Two-way repeated measures ANOVA, effect of interaction (genotype x time), $F_{(8,264)}$=3.18, P<0.01; Bonferroni multiple comparisons, *P<0.05, **P<0.01, ***P<0.001).

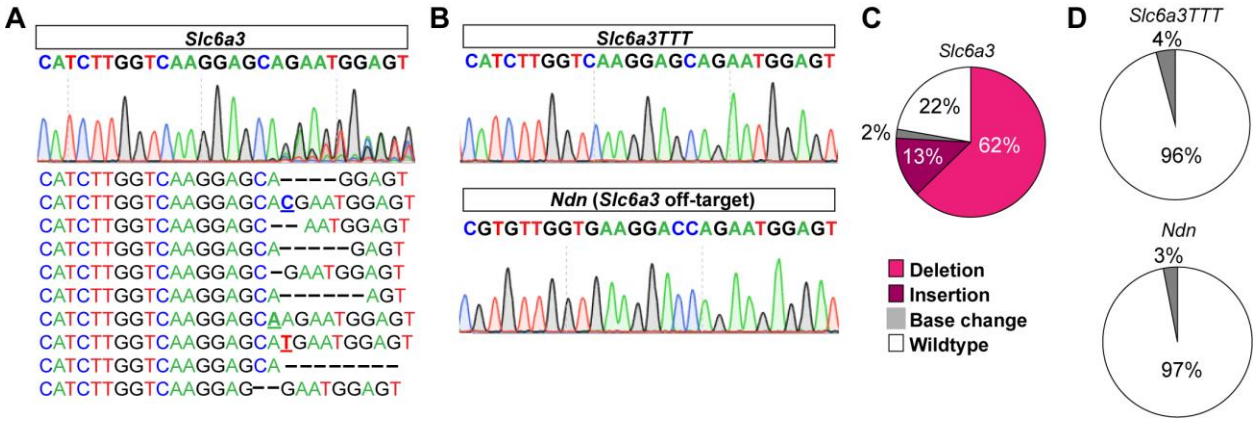

Figure 18: Confirmation of *Slc6a3* mutagenesis
Mice were co-injected with AAV1-FLEX-EGFP-KASH and AAV1-FLEX-SaCas9-sgSlc6a3 or AAV1-FLEX-SaCas9-sgSlc6a3TTT (controls). (A) Targeted Sanger sequencing of *Slc6a3* amplicons from GFP+ nuclei with the top 10 mutations observed in targeted deep sequencing. (B) Targeted Sanger sequencing of (top) *Slc6a3* amplicons from GFP+ nuclei from sgSlc6a3TTT mice and (bottom) CRISPOR predicted off-target *Ndn* amplicons from GFP+ nuclei from sgSlc6a3 mice. (C-D) Types of mutations observed from targeted deep sequencing of (C) *Slc6a3*, (D) *Slca63* (sgSlc6a3TTT mice), and *Ndn* amplicons from GFP+ nuclei.

CHAPTER 6: A FLP-DEPENDENT AAV-CRISPR/SACAS9 YIELDS EFFICIENT GENE INACTIVATION

Introduction

In addition to Cre-driver mouse lines, there is an emergence of mouse lines expressing the optimized yeast recombinase FlpO that recognizes FRT sites on DNA (Dymecki, 1996) that can be utilized for genetic manipulation (Sadowski, 1995). To determine whether SaCas9-mediated mutagenesis can be combined with Flp-mediated recombination, we generated AAV1-CMV-FLEXfrt-SaCas9-U6-sgRNA. To test the efficiency of AAV1-CMV-FLEXfrt-SaCas9-U6-sgRNA, we subcloned the guide for targeting *Grin1* (**Figure 19A**), the gene encoding the essential NR1 subunit of the NMDA receptor.

Sequencing verification of mutagenesis

Genetic inactivation of *Grin1* in dopamine neurons has been previously shown to eliminate NMDA receptor-mediated current in these cells (Engblom et al., 2008; Zweifel et al., 2008). Analysis of evoked excitatory postsynaptic currents (EPSCs) in fluorescently identified dopamine neurons through co-expression of AAV1-CAG-FLEXfrt-mCherry and AAV1-CMV-FLEXfrt-SaCas9-U6-sgGrin1 in Th-Flp mice (Poulin et al., 2018) revealed significantly reduced NMDAR-mediated EPSCs relative to AMPA-type glutamate receptor EPSCs in VTA dopamine neurons compared to either wild type dopamine neurons, or dopamine neurons transduced with the control virus AAV1-CMV-FLEXfrt-SaCas9-U6-sgGrin1ATG (**Figure 19B-D**).

Consistent with other genes mutated with Cre-dependent CRISPR/SaCas9, Flp-dependent CRISPR/SaCas9 targeting of *Grin1* resulted in a ~83% reduction in NMDAR function (91% mean reduction in 9 of 10 cells and no reduction in 1 of 10 cells).

In accordance with this, deep sequencing of amplicons from WGA FACS DNA extracted from GFP+ nuclei resulted in 72% mutagenesis (**Figure 22A-C**). Thus, AAV1-CMV-FLEXfrt-SaCas9-U6-sgRNA can also be used for *in vivo* gene mutagenesis.

Figure 19

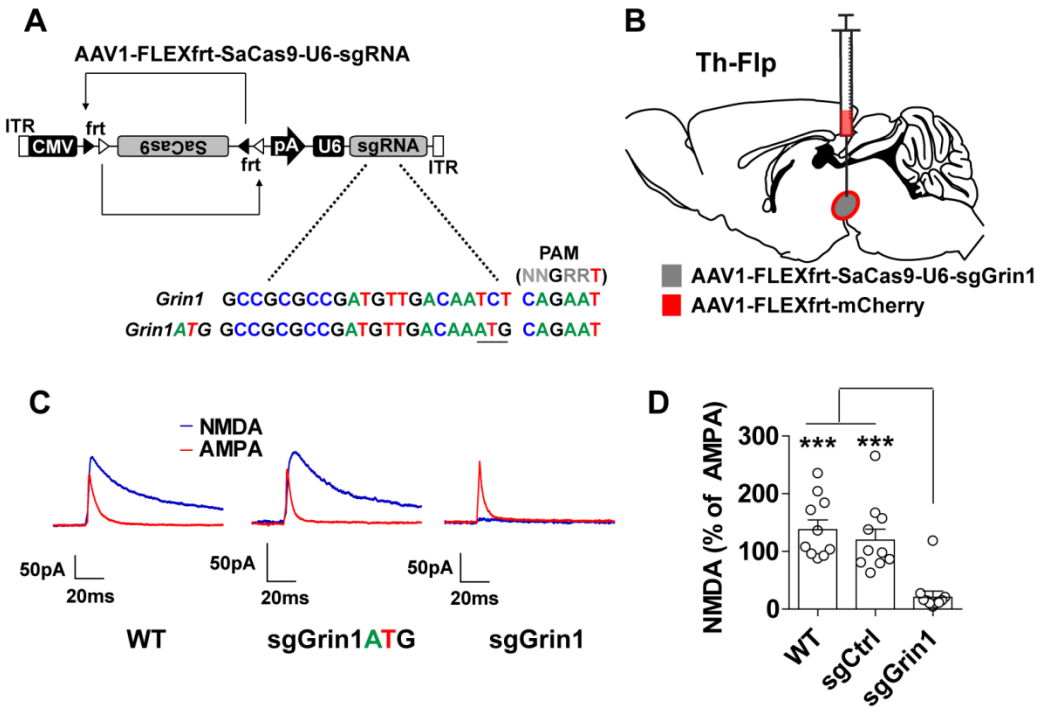

Figure 19: Flp-dependent CRISPR/SaCas9 is efficacious for gene mutagenesis
(A) Design of AAV1-FLEXfrt-SaCas9-U6-sgGrin1 and control virus AAV1-FLEXfrt-SaCas9-U6-sgGrin1ATG. (B) Illustration of sagittal section with viral injections into the VTA. (C) Representative traces of NMDA and AMPA currents evoked in dopamine neurons by electrical stimulation in WT mice or mice expressing sgGrin1 or sgGrin1ATG. AMPA current recordings were made in the presence of AP5; NMDA currents were determined by subtracting the AMPA current from the compound current trace recorded in ACSF. (D) Quantification of the peak NMDA current as a percent of the peak AMPA current (n=10 cells/group; One-way ANOVA $F_{(2,27)}$=15.55, P<0.0001; Tukey's multiple comparisons test ***P<0.001).

CHAPTER 7: LIBRARY OF PLASMID CONSTRUCTS FOR VIRAL CRISPR/SACAS9 GENE KNOCKOUT

Introduction

We have shown that AAV1-CMV-FLEX-SaCas9-U6-sgRNA is highly effective for mutagenesis and inactivation of dopamine and GABA-related neurotransmitter signaling using Cre-driver lines. Based on the success of inactivation of *Th* and *Slc6a3*, we generated a library of AAV1-CMV-FLEX-SaCas9-U6-sgRNA constructs for targeting vesicular glutamate transporters Vglut1, Vglut2, and Vglut3 (*Slc17a7, Slc17a6,* and *Slc17a3*), the vesicular GABA and glycine transporter Vgat (*Slc32a1*), and the vesicular monoamine transporter Vmat2 (*Slc18a2*) (**Figure 20**) to facilitate the cell-specific study of glutamate, GABA, and monoamine neurotransmission. In addition, based on the effective mutagenesis and inactivation of *Gabrg2*, we generated targeting viruses for other major ionotropic glutamate and GABA receptors (*Gria1, Gria2, Gria3, Grin1, Grin2a, Grin2b, Gabrg1,* and *Gabrg3*) (**Figure 20**). And lastly, based on the successful inactivation of *Grin1* with AAV1-CMV-FLEXfrt-SaCas9-U6-sgGrin1, we generated a second library of Flp-dependent constructs for targeting glutamatergic and GABAergic signaling using the same sgRNAs as the Cre-dependent constructs.

Strategy for validation of sgSlc17a7, sgSlc17a6, and sgSlc32a1

To determine the functionality of these constructs, we tested sgSlc17a7 (Vglut1), sgSlc17a6 (Vglut2), and sgSlc32a1 (Vgat) using channel rhodopsin (ChR2) and slice electrophysiology (**Figure 21**). To determine if targeting *Slc32a1* using sgSlc32a1

inhibited GABAergic signaling, we co-injected AAV1-FLEX-ChR2-YFP and either AAV1-CMV-FLEX-SaCas9-U6-sgSlc32a1 or AAV1-CMV-FLEX-SaCas9-U6-sgRosa26 (controls) into the lateral preoptic area (LPO) and AAV1-FLEX-mCherry into the VTA of Vgat-Cre mice. The LPO sends strong GABAergic projections to GABA neurons in the VTA, and Vgat is required for packaging GABA into vesicles for release into the synapse (Chaudhry et al., 1998; Saito et al., 2013). Stimulating ChR2 from terminals in the VTA from sgSlc32a1-targeted mice should result in lower amplitude IPSCs in GABA cells in the VTA compared to controls. As predicted, the amplitude of optically evoked IPSCs was significantly reduced in mCherry-positive (GABA neurons) cells relative to controls (**Figure 21B-D**).

Vglut1 and Vglut2 are both vesicular transporters that package glutamate into vesicles for synaptic release, but their expression patterns differ in the brain (Fremeau et al., 2001). Therefore, independently targeting either *Slc17a7* or *Slc17a6* in locations where they are expressed will inhibit glutamate signaling. Vglut1 is highly expressed in the prefrontal cortex (PFC) with the absence of Vglut2 expression (Fremeau et al., 2001). To validate the sgRNA targeting Vglut1 (sgSlc17a7), AAV1-FLEX-ChR2-YFP and either AAV1-CMV-FLEX-SaCas9-U6-sgSlc17a7 or AAV1-CMV-FLEX-SaCas9-U6-sgRosa26 (controls) were co-injected into the PFC of Vglut1-Cre mice. Optically evoked EPSCs in cells with dense ChR2 innervation in the central medial thalamus (CM) were measured. Relative to controls, sgSlc17a7-targeted mice had reduced EPSCs, suggesting gene mutagenesis and loss of glutamate signaling (**Figure 21E-G**).

In contrast, glutamate neurons in the pedunculopontine tegmental nucleus (PPTg) express Vglut2 and not Vglut1 (Fremeau et al., 2001). To determine if targeting

Slc17a6 resulted in reduced glutamatergic signaling, AAV1-FLEX-ChR2-YFP and either AAV1-CMV-FLEX-SaCas9-U6-sgSlc17a6 or AAV1-CMV-FLEX-SaCas9-U6-sgRosa26 (controls) were co-injected into the PPTg of Vglut2-Cre mice. Patching neurons with dense ChR2 innervation in the VTA resulted in a significant reduction in EPSC amplitude compared to controls (**Figure 21H-J**), demonstrating targeting *Slc17a6* in the PPTg inhibits glutamate signaling.

Sequence verification of mutagenesis

To confirm gene mutagenesis for these sgRNAs, Vgat-Cre, Vglut1-Cre, and Vglut2-Cre mice were co-injected with AAV1-FLEX-EGFP-KASH and the AAV expressing the corresponding sgRNA. WGA was performed on genomic DNA from sorted GFP+ nuclei. Amplicons were prepared to span the targeted region for each gene, and Sanger and deep sequencing were completed (**Figure 22D-J**). All three sgRNAs produced robust, targeted gene mutagenesis, further demonstrating the effectiveness of this viral-mediated CRISPR/SaCas9 approach.

Figures 20-22

Gene	sgRNA sequence	PAM (NNGRRT)
Slc17a7	CCACCATGGAGTTCCGGCAGG	AGGAGT
Slc17a6	TATGCTGATCCCATCTGCAGC	CAGAGT
Slc17a8	TACCCTGCCTGCCATGGGATG	TGGAGT
Slc18a2	CGATGAACAGGATCAGCTTGC	GCGAGT
Slc32a1	AGGAGCGCCGCCGCGCTGATA	ATGAAT
Grin1	GCCGCGCCGATGTTGACAATCT	CAGAAT
Grin2a	GAGCAGGCAACCGGCTTGCCC	CTGGAT
Grin2b	CACTTCGTCGGAAGTGCCCAC	GAGGAT
Gria1	ACATTCTAACAACCACGGAGG	AAGGAT
Gria2	TATTTCCAAGGGGCGCTGATC	AAGAAT
Gria3	GTGTTCATTGACATCTGGTCA	TAGAAT
Gabrg1	TGGGTAGAGCGATAGCAGGAG	AGGAGT
Gabrg2	GTGGGTAGAGCGATAGCAGGAG	CAGAAT
Gabrg3	AGACCCACTTCTGGTTTGATG	GGGAGT

Figure 20: Table of GABA and glutamate related genes with targeted sgRNAs cloned into the FLEX and FLEXfrt vectors.

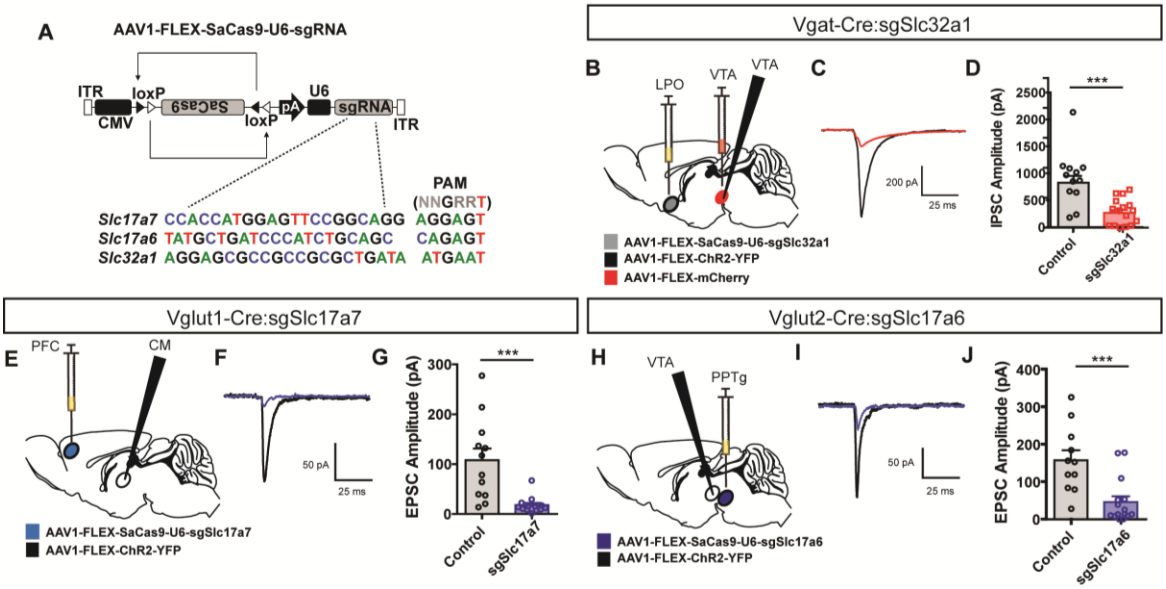

Figure 21: Testing of sgRNAs targeting GABA and glutamate transporters
(A) Design of AAV1-FLEX-SaCas9-U6-sgSlc17a7, AAV1-FLEX-SaCas9-sgSlc17a6, and AAV1-FLEX-SaCas9-sgSlc32a1. (B-D) Validation of sgSlc32a1. (B) Illustration of sagittal section with co-injection of AAV1-FLEX-SaCas9-sgSlc32a1 and AAV1-FLEX-ChR2-YFP into the lateral preoptic (LPO) and AAV1-FLEX-mCherry into the VTA of Vgat-Cre mice. (C) Representative traces of optically evoked IPSCs in mCherry-positive neurons in the VTA. (D) Quantification of IPSC amplitude in sgSlc32a1-targeted and control mice (Student's t test ***P<0.001). (E-G) Validation of sgSlc17a7. (E) Illustration of sagittal section with co-injection of AAV1-FLEX-SaCas9-sgSlc17a7 and AAV1-FLEX-ChR2-YFP into the PFC Vglut1-Cre mice. (F) Representative traces of optically evoked EPSCs in the central medial thalamus (CM). (G) Quantification of EPSC amplitude in sgSlc17a7-targeted and control mice (Student's t test ***P<0.001). (H-J) Validation of sgSlc17a6. (H) Illustration of sagittal section with co-injection of AAV1-FLEX-SaCas9-sgSlc17a7 and AAV1-FLEX-ChR2-YFP into pedunculopontine tegmental nucleus (PPTg) of Vglut2-Cre mice. (I) Representative traces of optically evoked EPSCs in the VTA. (J) Quantification of EPSC amplitude in sgSlc17a6-targeted and control mice (Student's t test ***P<0.001).

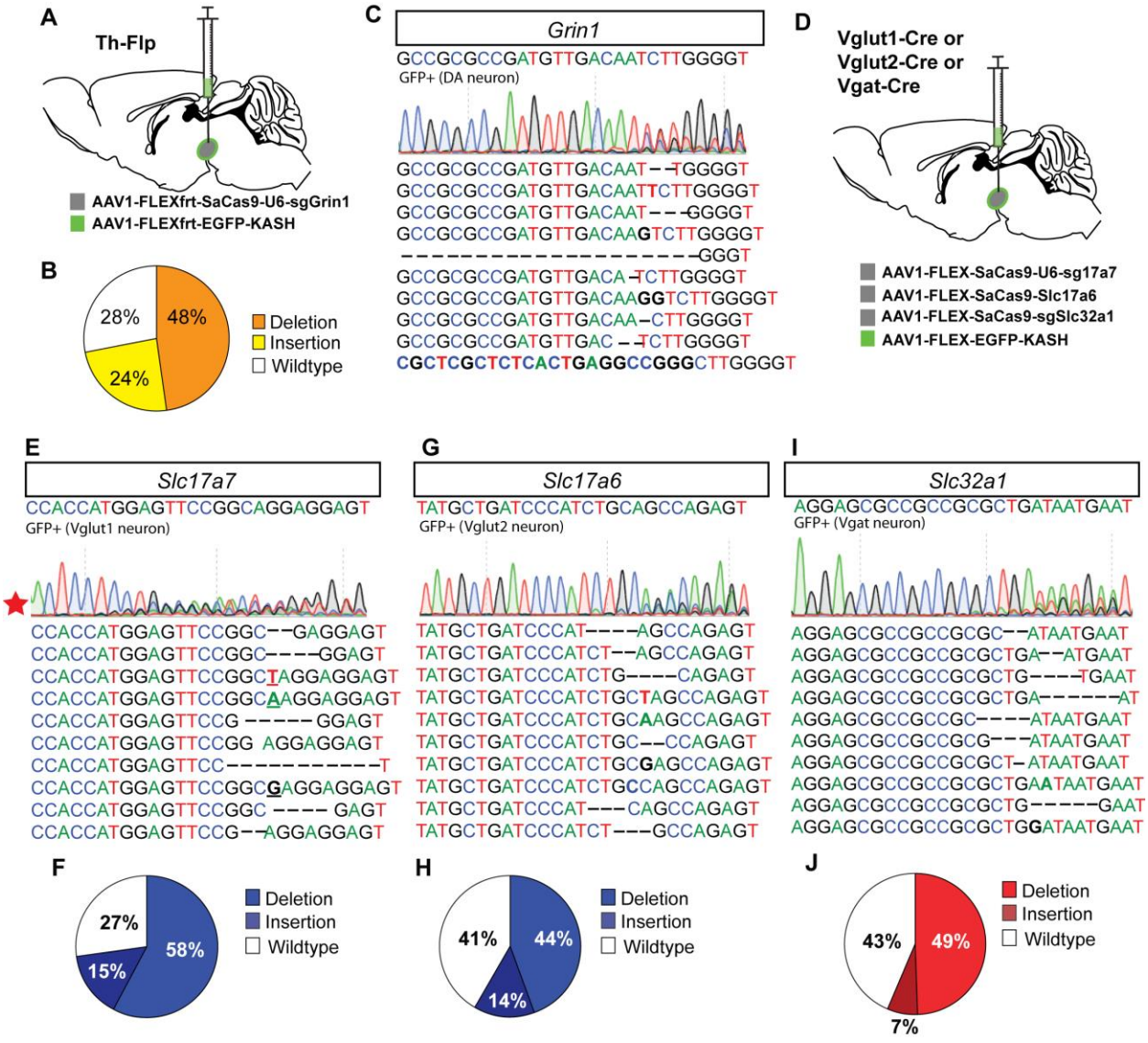

Figure 22: Sequencing results confirm gene mutagenesis of *Grin1*, *Slc17a7*, *Slc17a6*, and *Slc32a1*
(A-C) Mice were co-injected with AAV1-FLEX-EGFP-KASH and AAV1-FLEX-SaCas9-sgGrin1. (A) Illustration of sagittal section with viral injections into the VTA. (B) Types of mutations observed from targeted deep sequencing of *Grin1*. (C) Targeted Sanger sequencing of *Grin1* amplicons from GFP+ nuclei with the top 10 mutations observed in targeted deep sequencing. (D) Illustration of sagittal section with viral injections into the VTA. (E-F) Amplicons from GFP+ nuclei from mice co-injected with AAV1-FLEX-EGFP-KASH and AAV1-FLEX-SaCas9-sgSlc17a7. Star indicates Sanger sequencing was completed using the reverse primer (see methods). (E) Targeted Sanger sequencing of *Slc17a7* amplicons with the top 10 mutations observed in deep sequencing. (F) Types of mutations observed from targeted deep sequencing of *Slc17a7*. (G-H) Amplicons from GFP+ nuclei from mice co-injected with AAV1-FLEX-EGFP-KASH and AAV1-FLEX-SaCas9-sgSlc17a6. (G) Targeted Sanger sequencing of *Slc17a6* amplicons with the top 10 mutations observed in deep sequencing. (H) Types of mutations observed from targeted deep sequencing of *Slc17a6*. (I-J) Amplicons from GFP+ nuclei from mice co-injected with AAV1-FLEX-EGFP-KASH and AAV1-FLEX-SaCas9-sgSlc32a1. (I) Targeted Sanger sequencing of *Slc32a1* amplicons with the top 10 mutations observed in deep sequencing. (J) Types of mutations observed from targeted deep sequencing of *Slc32a1*.

CHAPTER 8: DISCUSSION

We have demonstrated that a single viral vector for the recombinase-dependent expression of SaCas9 and a single sgRNA is sufficient for generating genetic LOF and successive phenotypic analysis. We have validated this technique by targeting 9 different genes of diverse function in distinct cell types and performed an array of analyses to confirm gene mutagenesis and subsequent protein loss, including IHC, FACS and sequencing, electrophysiology, Western blots, and behavior. We have shown in multiple experiments that AAV1-CMV-FLEX-SaCas9-U6-sgRNA is as efficacious as conventional Cre/loxP gene inactivation using floxed mouse lines through either a breeding strategy or through viral Cre delivery. We demonstrated the additional benefits of targeting gene mutagenesis and inactivation in cell types previously difficult to isolate for gene inactivation, and show the effectiveness of this strategy for projection-specific targeting using an intersectional approach. Lastly, we validated sgRNAs that can be used to target vesicular glutamate and GABA transporters to enhance the study of neural signaling in the brain. Thus, the use of AAV1-CMV-FLEX-SaCas9-U6-sgRNA provides a valuable strategy for rapid, efficient and robust analysis of gene function.

A major consideration for the use of AAV1-FLEX-SaCas9-U6-sgRNA is the selection of controls to account the expression of SaCas9, the ubiquitous expression of the sgRNA, and potential off-target effects. We considered several approaches to address this, including the design of guides that target noncoding DNA within the mouse genome to control for the expression of SaCas9, injection of AAV1-CMV-FLEX-SaCas9-U6-sgRNA into wild type mice to control for viral transduction and constitutive

expression of the targeting sgRNA, designing an sgRNA that still produced double strand breaks but had no effect on cellular function, and mutating regions of the sgRNA to maintain the same potential off-targets as the chosen guide. The most rigorous control would be the re-expression of the target gene through viral delivery of an open reading frame in which DNA sequence corresponding to the sgRNA is modified to encode the same amino acids but with different codons not targeted by the guide. The major limitations to this approach are the time and expense of generating cDNA for viral re-expression, the open reading frame of some genes is too large to package into an AAV, and overexpression of the targeted gene may in itself confer a change in cellular physiology.

Based on these considerations, we designed two types of sgRNA controls. The first was a control that produced gene mutagenesis in *Rosa26*, a locus that is regularly used for gene insertions and does not have any known function but is transcribed. Secondly, we generated sgRNAs containing a 3 base mutation within the important sgRNA seed region. The mutated sgRNA guide is 85% identical to the sgRNA of interest, which controls for the expression of SaCas9 and its potential off target actions. We tested this strategy multiple times and observed that the control guides do not mutate the gene of interest and do not alter protein levels associated with the gene product. We conclude that either the sgRosa26 or sgGeneTTT control would be sufficient for future studies.

In addition to the selection of controls, an equally important consideration is the selection of the sgRNA. Using the simple strategy which sgRNAs were targeted to the most 5’ conserved exon, we routinely and consistently achieved efficiency that was

equivalent to conventional gene knockout. In 9 of 9 targeted genes, the first guide we chose based on this criterion was highly effective. In addition to the 9 gene targets described here, we have also successfully targeted +30 other independent genes encoding a variety of ion channels, synaptogenic proteins, and G-protein coupled receptors using this strategy. In all cases, we observe highly efficient gene mutagenesis and inactivation with the selection of a single sgRNA.

We found high rates of gene mutagenesis in every sgRNA tested. We showed that ~90% of the brightest GFP+ cells contained targeted gene mutagenesis, demonstrating that appropriate methodology for analyzing mutagenesis is critical for accurately reporting mutation rates. Past experiments determining CRISPR/Cas mutations have found considerably lower gene mutagenesis rates than reported here (Fu et al., 2013; Kim et al., 2015; Kim et al., 2017; Kumar et al., 2018; Tsai et al., 2015). However, these studies used genomic DNA from cells either transduced in culture (Fu et al., 2013; Kim et al., 2015; Kim et al., 2017; Tsai et al., 2015) or from an entire tissue punch in the brain (Kumar et al., 2018) for gene mutagenesis confirmation. Viral spread in tissue is restricted to the anatomical location injected, and obtaining a punch that only contains virus-infected cells is nearly impossible. Furthermore, cellular mechanics in culture are highly different from neurons *in vivo*, so even if cell transfection rates are robust, drawing parallels between them may be insufficient. Thus, we conclude sorting GFP+ nuclei from mice via FACS is the best method for analyzing gene mutagenesis caused by Cas9 cleavage.

Our method presented an average of 61% of reads with mutations using the larger, combined gate. Analysis of targeted deep sequencing data revealed all genes

mutated presented more deletions than insertions, with an average deletion occurrence of 3.5x more than an insertion (**Figure 23**). In addition, 74% of mutations resulted in a frameshift suggesting a repair from CRISPR/Cas cleavage is 3x more likely to produce a frameshift than an in-frame mutation. Base changes were present in an average of less than 2% of reads. Interestingly, while all TTT controls and predicted off-targets *Wdfy3* (*Gabrg2*), *Socs6* (*Kcnn3*), and *Ndn* (*Slc6a3*) exhibited less than 4% mutation rate, *Paxbp1* (*Gabrg2*) had a 12% mutation rate in sgGabrg2-targeted cells. *Paxbp1* (also known as *GCFC1*) encodes the PAX3 and PAX7 binding protein 1, which is a ubiquitously expressed transcription factor (Mohammadparast et al., 2014). Analysis of the types of mutations reveals that over half (6.5%) of these mutations are single base changes, while the other 5.5% are deletions. The off-target cleavage site in *Paxbp1* is located at the 3' end of exon 11 (out of 18 total exons) and between codons for amino acids P641 and L642 (919 amino acids total) (Kent et al., 2002). Even if these deletions were deleterious to the function or expression of *Paxbp1*, we believe a 5.5% deletion rate is within reasonable range and should not influence the behavioral phenotypes observed.

Use of AAV1-CMV-FLEX-SaCas9-U6-sgRNA has distinct advantages over other methods. Because the SaCas9 and sgRNA are packaged within a single vector, the delivery is not subject to confounds of using viral vectors of different serotypes, or the generation of two independent viral vectors of the same serotype that may differ in effective titer. Conventional gene inactivation requires the generation of a conditional allele, backcrossing, and crossing to a recombinase driver line of interest that can take years before testing. In contrast, conceptualization of the gene to target in a specific cell

type or circuit connection to sgRNA cloning, to viral production, to in vivo analysis using AAV1-CMV-FLEX-SaCas9-U6-sgRNA and AAV1-CMV-FLEXfrt-SaCas9-U6-sgRNA can be achieved in less than two months. Moreover, the ability to restrict gene mutagenesis and protein loss to adult mice avoids technical confounds such as ectopic germline expression of the recombinase, or early developmental expression that is not restricted to the cell line of interest. This method also presents an advantage over the Cre-dependent SpCas9 mouse lines by reducing the need for additional breeding as the virus can be injected directly into Cre or Flp driver lines of interest, and avoids the potential confounds of developmental recombinase expression. An additional benefit of SaCas9 conditionally expressed by either Cre or Flp recombinase is that cell-type specific Cre and Flp driver lines can be crossed to generate compound heterozygotes and different genes in different cell types can be inactivated to test for transcellular genetic interactions.

Using the AAV1-CMV-FLEX-SaCas9-U6-sgRNA, we were able to target cells that are challenging to genetically manipulate using conventional strategies that allowed us to address previously unanswerable questions. GABAergic signaling has been show to play an important role in behavioral sensitization to cocaine (Edwards et al., 2017) but the contribution of $GABA_A$ receptor signaling in GABAergic neurons of the VTA has been difficult to assess. Using AAV1-CMV-FLEX-SaCas9-U6-sgGabrg2, we were able to show that a significant reduction in synaptic $GABA_A$ signaling on GABAergic but not dopaminergic neurons in the VTA is sufficient to reduce psychomotor sensitization to cocaine. Thus, single vector SaCas9-mediated mutagenesis can be utilized to establish novel genotype-phenotype interactions with cellular and anatomical specificity. We

found that significantly reducing fast synaptic GABA transmission on dopamine neurons had no overt phenotype or effects on cocaine sensitization. These results are consistent with previous reports demonstrating that reducing fast GABA transmission through the inactivation of the $GABA_A$ receptor β3 subunit has no effects on basal locomotor activity (Parker et al., 2011). These results are also in agreement with recent observations that $GABA_B$ receptor signaling on dopamine neurons is a key regulator of psychomotor sensitization to cocaine (Edwards et al., 2017). Together with our results these findings suggest that the coordinate actions of $GABA_B$ receptors on dopamine neurons and $GABA_A$ receptors on GABAergic neurons of the VTA contribute to this behavioral phenomenon. Through our demonstration of the effectiveness of the FLP-dependent AAV1-CRISPR/SaCas9 system, future experiments utilizing a combination of Th-Flp and Vgat-Cre, or Vgat-Flp and DAT-Cre mice to target different GABA receptors in distinct cell types will now be feasible.

Viral-mediated CRISPR/SaCas9 provides an efficient means for intersectional targeting of projection populations. It was previously demonstrated that SaCas9 packaged into a retrograde AAV (AAV2-Retro) was effective at silencing ectopic tdTomato reporter expression in mice (Tervo et al., 2016). The disadvantage of the non-conditional AAV2-Retro-SaCas9 is that it does not restrict mutagenesis to a single anatomical input region, though it does have other distinct advantages. Using the intersectional strategy described here, we were able to demonstrate the effectiveness of circuit-level analysis of gene inactivation. It has been previously demonstrated that loss of DAT in mice results in hyperactivity and a reduced responsiveness to cocaine (Giros et al., 1996). Whether these effects are mediated by the loss of DAT in

mesoaccumbens dopamine neurons or nigrostriatal dopamine neurons was not previously easy to address. By selectively targeting *Slc6a3* in VTA dopamine neurons, or in VTA projections to the NAc, we were able to demonstrate that loss of DAT in the mesoaccumbens pathway is sufficient to cause hyperactivity. Interestingly, this manipulation did not result in an initial loss of psychomotor activation in response to cocaine but rather desensitization over consecutive days. Thus, nigrostriatal DAT inhibition by cocaine or some combination of nigrostriatal dopamine and mesoaccumbens dopamine is required for the initial sensitivity to this drug.

Based on our collective observations, we conclude that the addition of AAV1-FLEX-SaCas9-U6-sgRNA to the genetic toolbox provides a highly reliable and efficient means for generating gene knockout models, furthering our capacity for genetic and cellular isolation to probe gene function in the regulation of the central nervous system.

Figure 23

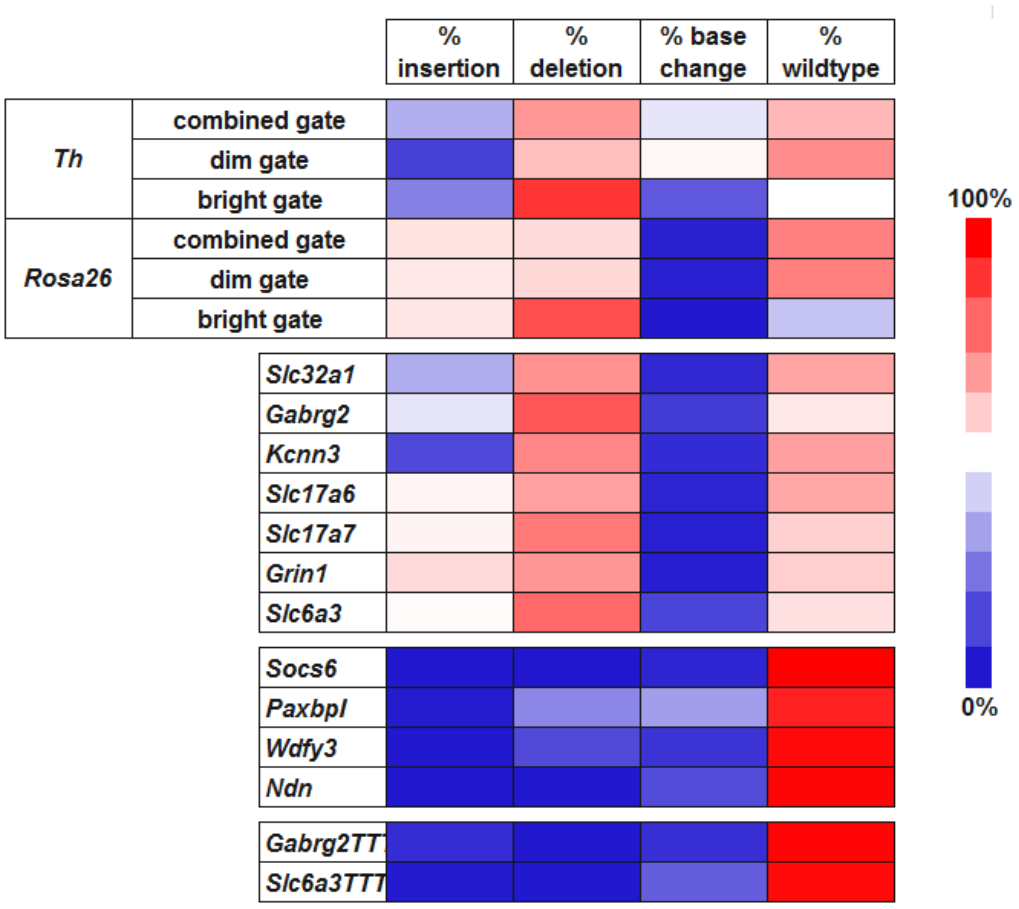

Figure 23: Heat map of mutations observed from deep sequencing of CRISPR/SaCas9 targeted loci

CHAPTER 9: FUTURE DIRECTIONS

Introduction

The CRISPR/Cas9 strategy described in this study exploits the NHEJ cellular repair pathway to induce genomic mutagenesis *in vivo*. This straightforward knockout strategy has unlocked the ability to perform previously unfeasible reverse genetic studies. With the advent of new CRISPR/Cas9 technology such as a Cas9 nickase (Cas9n)(Cong et al., 2013), a catalytically inactive Cas9 (dCas9)(Fernandes et al., 2019), and prime editing used in combination with a reverse transcriptase (Anzalone et al., 2019), the field of CRISPR/Cas9 applications has expanded even further. These new developments allow for more specific mutations, gene activation and suppression rather than knockout, insertion of large genes into specific loci, temporal control of CRISPR/Cas9 using drugs or exploiting the use of anti-CRISPR proteins to inactivate Cas9 *in vivo*.

Gene activation/suppression by CRISPRa and CRISPRi

Inducing or inhibiting gene expression is an attractive alternative to producing pseudo-random indel mutations. CRISPRa and CRISPRi are methods for gene activation and interference, respectively, using a catalytically inactive Cas9 (dCas9) (Fernandes et al., 2019; Gilbert et al., 2013; Larson et al., 2013; Qi et al., 2013). CRISPRi is achieved by fusing dCas9 to Kruppel-associated box (KRAB) domain to promote heterochromatin and consequently, inhibit gene expression. In HEK293 cell culture using a GFP reporter, CRISPRi can repress GFP fluorescence by 75% (Gilbert

et al., 2013). In contrast, when using dCas9 fused to transcription factors (either VP64 or VP160) for CRISPRa, only a modest increase in gene expression was observed *in vitro* (Gilbert et al., 2013).

Recently, however, CRISPRa was used to increase transcription of the α subunit of $Na_v1.1$ from the *Scn1a* locus in *Scn1a*$^{+/-}$ haploinsufficent mice (Colasante et al., 2019). Mutations in *Scn1a* cause Dravet syndrome, a type of infancy-onset epilepsy with autism and hyperactivity comorbidities (Dravet, 2011). Most patients with Dravet syndrome incur *Scn1a* mutations *de novo*, resulting in haploinsufficiency. Using databases with promoter information such as ENCODE, Colasante et al. tested multiple sgRNAs that targeted sequences in two different promoter regions near distinct transcriptional start sites (TSSs). When targeting the proximal promoter with CRISPRa, a 4-fold increase in *Scn1a* mRNA and a 2-fold increase in $Na_v1.1$ protein were observed. The CRISPRa-mediated enhanced $Na_v1.1$ expression was sufficient to restore neuronal excitability deficits observed in *Scn1a*+/- interneurons in mice. This study establishes that CRISPRa can address questions on gene expression sufficiency *in vivo*.

In addition to sufficiency studies, CRISPRa and CRISPRi could be used to test for possible compensation from other gene paralogues. This could be achieved by knocking out one gene using conventional CRISPR/Cas9 or Cre/LoxP, and then activating or inhibiting its paralogue with CRISPRa or CRISPRi, respectively. The ability to make these systems reversible by incorporating tetracycline-dependency through Tet-Off or Tet-On would further expand their possible uses.

To create a viral-mediated tetracycline-dependent CRISPRa or CRISPRi system, a single vector would contain a dCas9 fused to a Tet Response Element (TRE), a sgRNA designed to target a promoter region upstream of a TSS, and a tetracycline-controlled transactivator (tTA, fusion of the tet repressor with VP16, a transcription activator). Expression of these three components would (in theory) turn on gene expression in three sequential steps by 1) sgRNA guiding dCas9-TRE to promoter, 2) tTA binding to TRE on dCas9, and 3) tTA recruiting transcriptional machinery. Exposure to tetracycline would turn off expression via tetracycline binding to tTA, releasing tTA from the TRE, thereby evading recruitment of transcriptional machinery. One consideration is there may be steric hindrance of endogenous transcriptional machinery caused by dCas9 bound to the DNA, although it is unclear whether this would provide additional leveraging control or hinder regular gene activity in this inducible system.

Drug-dependent activation of SaCas9

Studies testing the necessity and sufficiency of genes within defined cell populations are critical to our understanding of the central nervous system. Currently, the capability to knockout and then overexpress specific genes must be completed in separate groups of mice. Controlling the activity of Cas9 to permit temporal regulation of gene mutagenesis would provide a powerful technique for studying the function of genes.

Kelkar et al. used the self-inactivating CRISPR (SiC) system to disable Cas9 in a deoxycycline-dependent manner (Kelkar et al., 2019). To do this, the sgRNA-Cas9 complex first performs gene mutagenesis. Next, upon doxycycline treatment, a second

sgRNA is transcribed which competes with the original sgRNA to bind Cas9 and effectively, inhibits further Cas9 activity.

For loss of function studies, it may be more effective to control the timing of Cas9-mediated gene mutagenesis rather than Cas9 inactivation. One idea would be to fuse SaCas9 to the mutated ligand binding domain of the estrogen receptor (SaCas9-ER^T). Only under tamoxifen administration would SaCas9-ER translocate to the nucleus and cleave the target DNA. Due to the size restrictions of the small AAV genome, this system would require dual plasmids, one for SaCas9-ER fusion protein, and a second for the U6 driven sgRNA. Using this strategy, the same group of mice could be tested before and after tamoxifen treatment (i.e. before and after gene mutagenesis, respectively) in a behavioral paradigm. This matched study design limits variance due to other factors, providing strong statistical evidence that the experimental variable is the cause of the behavioral phenotype observed.

Inhibition of Cas9 by anti-CRISPR proteins

CRISPR/Cas9 is an adaptive immune system used by bacteria and archaea to destroy foreign DNA from intruding viruses or bacteriophages. In some occurrences, the intruders are able to evade destruction through either rapid mutagenesis of the PAM or proto-spacer, or by expressing proteins that inhibit CRISPR machinery (anti-CRISPR proteins) during the interference step (Bondy-Denomy et al., 2013).

Structure-function analyses have revealed the actions of phage anti-CRISPR protein AcrIIA6 with *Streptococcus thermophilus* St1Cas9 (Fuchsbauer et al., 2019). Experiments using cryo-electron microscopy (cryo-EM) show that AcrIIA6 binds to the

backside of St1Cas9, resulting in self-dimerization of St1Cas9. In turn, this dimerization successfully blocks access of the catalytic domains to DNA, suggesting AcrIIA6 functions as an allosteric modulator. Further analysis of the AcrIIA6-St1Cas9 interaction using a biolayer interference assay demonstrates AcrIIA6 is slow to dissociate from St1Cas9, representing a quasi-irreversible bond. In contrast to the mechanism of St1Cas9 inhibition by AcrIIA6, AcrIICI is a broad spectrum Type II Cas9 inhibitor that binds to the HNH nuclease domain on Cas9 during the catalytically inactive state, but still permits DNA binding (Pawluk et al., 2016). Future studies could employ information gathered from anti-CRISPR protein mechanics to either block SaCas9 activity before or after mutagenesis by making this system doxycycline-dependent.

Multiplex genome editing using multiple Cas9 enzymes

Neurons are highly connected to other neurons in the CNS. Manipulation of a single gene within one cell type most likely has consequences on the physiology of other connecting cells. The ability to silence two different genes in two distinct cell types within an anatomical location would provide insight on how the expression of genes can alter network activity.

The high degree of diversity in CRISPR/Cas systems lends this as the perfect candidate for such studies. This could be accomplished by designing a triple vector system using both SpCas9 and SaCas9 in combination with a Flp-dependent and Cre-dependent mouse line. Co-injection of AAV-FLEX-SaCas9, AAV-FLEXfrt-SpCas9 and AAV-U6-sgRNA(SaCas9)-U6-sgRNA(SpCas9) into a Flp/Cre mouse line would restrict SpCas9 and SaCas9 expression to only Flp or Cre expressing cells, respectively. Due

to the unique scaffold architecture of the sgRNAs, each Cas9 requires its own distinctive sgRNA to be guided to PAM sequences on DNA. Using this vector system in combination with transgenic mice allows for isolation of gene mutagenesis to only cells with both the appropriate Cas9 and matching sgRNA expressed.

Gene insertions

The CRISPR/Cas9 method described here results in robust gene mutagenesis and subsequent loss of protein by activation of the NHEJ cell repair pathway. While this strategy is highly useful for protein knockout studies, the ability to create consistent and specific mutations would greatly expand the CRISPR/Cas9 toolbox. The less common homologous directed cell repair pathway (HDR) has the capacity to repair DNA precisely, but requires the use of a template. To shift the mode of repair *in vivo* from NHEJ to the preferred HDR, several studies have demonstrated creative methods for template delivery.

One such method for template delivery uses a dual AAV vector system, where one AAV contains Cas9 and the second comprises of the sgRNA and template (Nishiyama et al., 2017). The template (~4kb in length) has two long arms with sequences homologous to the target DNA surrounding an insertion. It is believed that packaging the template in an AAV facilitates HDR-mediated repair due to the single stranded nature of its genome, the delivery of the template directly to the nucleus, and the deposit of multiple plasmid copies per cell, increasing the template available for HDR (Russell and Hirata, 1998). Nishiyama et al. tested this method in vivo and found ~10-12% of virally transduced cells successfully repaired through HDR. One possible

explanation for the small percentage of HDR may be due to low concentration of template within the proximity of the Cas9 induced double strand DNA break.

To increase proximity of the template to the target location, there have been multiple attempts to link the template to either Cas9 or the sgRNA using protein-protein interactions. Carlson-Stevermer et al. connected a single stranded template to the stem loop on the sgRNA using a streptavidin-biotin interaction, but only observed 1.6% HDR (Carlson-Stevermer et al., 2017). Porcine cirovirus protein 2 (PCV) was used to covalently link the single stranded template to Cas9, and obtained as high as 20-30% HDR (Aird et al., 2018). However, in both studies, the RNA-Cas9-protein-DNA template complex requires *in vitro* assembly, limiting its possible applications.

New research has incorporated reverse transcriptases to increase the number of single stranded DNA template copies per cell. Cas9 Retron PrecISe Parallel Editing via homology (CRISPEY) utilizes retron elements that form an RNA scaffold for the *E. Coli* reverse transcriptase (RT Ec86) (Sharon et al., 2018). RT Ec86 uses a branching “G” on the RNA retron elements to synthesize single stranded DNA copies (msDNA) of the RNA template sandwiched between the retron elements (**Figure 24**). The retron elements are fused to the 5’ end of the sgRNA, permitting close proximity of the template to the Cas9 cleavage site. CRISPEY demonstrated close to 100% HDR when inserting EGFP into the genome of *Saccharomyces Cerevisiae* (*S. Cerevisiae*). However, *S. Cerevisiae* are notorious for using HDR in cell repair mechanisms much more frequently than mammalian systems (Coic et al., 2008). Therefore, it has yet to be determined whether this approach is even feasible in mammalian cells.

Prime editing is a new approach that also requires an RT. Prime editing uses Cas9n (Cas9 nickase) fused to an RT, which is guided to the genome by a prime editing guide RNA (pegRNA). The pegRNA consists of the sgRNA fused at the 3' end to a primer binding site and the reverse transcriptase template (which includes the desired DNA insertion) (Anzalone et al., 2019). When Cas9n nicks the DNA, it leaves a 5' and 3' flap hanging from the genomic DNA. The 3' flap is complementary to the primer binding site on pegRNA. The binding of the 3' flap to the primer binding site on the pegRNA initiates the RT to use the template to fill in the remaining bases including the desired mutation. This strategy successfully caused precise mutations in up to 65% of expressing HEK293 cells, but was much less efficacious in other cell types.

A few alterations to the previous approaches may increase the rate of precise gene insertions *in vivo*. One idea would be to express the retron elements, template, sgRNA, and reverse transcriptase on a bicistronic vector. A CMV promoter would drive the expression of the template, flanked by retron elements, and fused to the 3' end of the sgRNA, which has been shown to be more tolerant to cargo loading than the 5' end (Shechner et al., 2015). A second CMV promoter would transcribe the RT. The template would consist of two homology arms (~400bp each) flanking the desired insertion to permit larger DNA additions, such as genes expressing Cre or EGFP. A separate AAV would express SaCas9. Binding of the RT to the retron elements would initiate synthesis of msDNA from the RNA template. The msDNA template would then be in close proximity to repair the Cas9-cleaved genomic DNA, shifting the mode of cell repair from NHEJ to HDR by aligning the homology arms with the cleaved DNA and inserting the gene of interest in the exact locus desired (**Figure 24**).

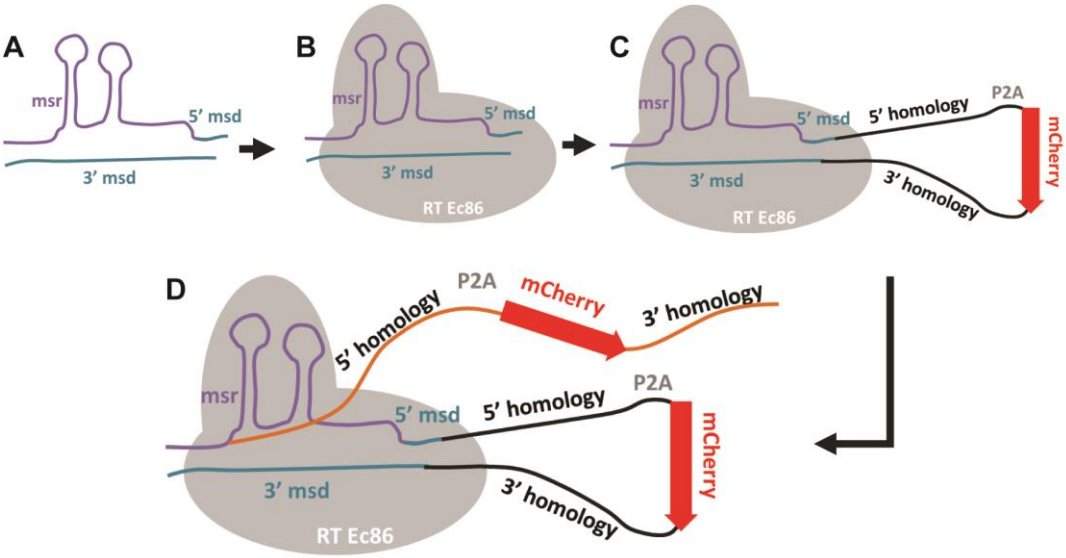

Figure 24: Diagram of msDNA synthesis from a template by RT Ec86
(A) Components of the retron element for the msRNA (msr) and the msDNA (msd). (B) RT Ec86 binds to the retron elements. (C) Diagram of a potential template containing mCherry flanked by homology arms inserted between the 5' and 3' msd. (D) Synthesis of the msDNA from the inserted template.

Concluding remarks

The high specificity, ease, and adaptability of CRISPR/Cas editing render it an immensely powerful gene mutagenesis tool. The applications of CRISPR/Cas are not limited to the ones discussed in this study: future research fine tuning and adjusting these approaches will further expand the applicability of CRISPR/Cas. We are just in the beginning!

CHAPTER 10: EXPERIMENTAL METHODS

Experimental Model and Subject Details.

All mice are on a C57BL/6J background. The Slc6a3$^{Cre/+}$ mouse line was generated as described (Zhuang et al., 2005), and the Slc32a1$^{Cre/+}$, Slc17a7 $^{Cre/+}$, and Slc17a6 $^{Cre/+}$ mouse lines were acquired from Jackson Laboratories (stock numbers 016962, 023527, and 028863, respectively). Th$^{Flp/+}$ mice were kindly given by Dr. Rajeshwar Awatramani (Poulin et al., 2018). Kcnn3$^{lox/lox}$ mice were generously provided by Dr. John Adelman (Jackson stock number 019083). The Kcnn3$^{\Delta}$ allele was generated by crossing Kcnn3$^{lox/lox}$ mice with a ubiquitously expressed Cre (Mox2$^{Cre/+}$). Slc6a3$^{Cre/+}$; Kcnn3$^{\Delta/+}$ mice were crossed with Kcnn3$^{lox/lox}$ mice to generate Slc6a3$^{Cre/+}$; Kcnn3$^{lox/+}$ (heterozygous for *Kcnn3* in dopamine neurons) and Slc6a3$^{Cre/+}$; Kcnn3$^{lox/\Delta}$ (Kcnn3 knockout in dopamine neurons).

Mice were group-housed (max 5 mice/cage) on a twelve-hour light/dark cycle with ad libitum access to food and water. All experiments were performed during the light phase in accordance with the Institutional Animal Care and Use Committee at the University of Washington. Equal numbers of male and female mice were used in each experiment. Mice were 3-6 months old for behavioral experiments and immunohistochemistry, 8-10 weeks old for slice electrophysiology, and 3-4 months old for FACS analysis.

Selection and design of sgRNAs.

The full length sequence for every gene was found on the UCSC genome browser database (*http://genome.ucsc.edu/*) (Kent et al., 2002), and the exons and splice

isoforms of each gene were identified and aligned (Mouse Genome Informatics (MGI) database) (Bult et al., 2019). The most 5' common coding exon (present in all known splice isoforms) was selected and the sequence was uploaded to the CRISPOR website (crispor.tefor.net) to determine possible sgRNAs and PAM sequences. The final sgRNA was chosen based on specificity, probability of frameshift mutations, and location on exon. Each sgRNA was ordered as short oligos (Sigma) with a 5' CACC- 3' overhang on the forward primer, and a 5' AAAC 3' overhang on the reverse primer to allow for seamless integration into the AAV1-FLEX-SaCas9-sgRNA vector (Table 1).

Table 1

Gene	**Oligos ordered for sgRNAs**
Th	Forward: 5' CACCGCCAAGGTTCATTGGACGGCGG 3' Reverse: 5' AAACCCGCCGTCCAATGAACCTTGGC 3'
Gt(Rosa26)Sor	Forward: 5' CACCGCTCGATGGAAAATACTCCGAG 3' Reverse: 5' AAACCTCGGAGTATTTTCCATCGAGC 3'
Slc6a3	Forward: 5' CACCGCATCTTGGTCAAGGAGCAGAA 3' Reverse: 5' AAACTTCTGCTCCTTGACCAAGATGC 3'
Kcnn3	Forward: 5' CACCGTTCTGGGCACTTCCATGACTC 3' Reverse: 5' AAACGAGTCATGGAAGTGCCCAGAAC 3'
Gabrg2	Forward: 5' CACCGTGGGTAGAGCGATAGCAGGAG 3' Reverse: 5' AAACCTCCTGCTATCGCTCTACCCAC 3'
Slc32a1	Forward: 5' CACCGAGGAGCGCCGCCGCGCTGATA 3' Reverse: 5' AAACTATCAGCGCGGCGGCGCTCCTC 3'
Slc17a7	Forward: 5' CACCGCCACCATGGAGTTCCGGCAGG 3' Reverse: 5' AAACCCTGCCGGAACTCCATGGTGGC 3'
Slc17a6	Forward: 5' CACCGTATGCTGATCCCATCTGCAGC 3' Reverse: 5' AAACGCTGCAGATGGGATCAGCATAC 3'
Grin1	Forward: 5' CACCGCCGCGCCGATGTTGACAATCT 3' Reverse: 5' AAACAGATTGTCAACATCGGCGCGGC 3'

Cloning sgRNAs into pAAV1-FLEX-SaCas9-sgRNA.

The pAAV1-FLEX-SaCas9-sgRNA plasmid was digested overnight with BsaI-HFv2 and gel purified (Qiaquick Gel Extraction Kit, Qiagen). The ordered sgRNA oligos were resuspended to a concentration of 100uM. The oligos were phosphorylated at 37°C for

30min using the following reaction: 1uL of each oligo, 1uL T4 ligase buffer (NEB), 0.5uL phosphonucleotide kinase (PNK, NEB) and 6.5uL H2O. To anneal the oligos, the entire reaction was placed at 100°C for 5 minutes and allowed to slowly return to room temperature. 50ng of digested pAAV-FLEX-SaCas9-sgRNA and 1uL T4 ligase (NEB) were added directly to the reaction and incubated at room temperature for 2 hours. 2uL of the reaction was next electroporated using DBH10 beta electrocompetent cells (NEB). Colonies were grown in LB + AMP and minipreps (Qiagen) were performed to extract DNA. A restriction digest using BsaI-HFv2 and HindIII-HF was performed to screen for positive colonies. One positive colony was selected and the DNA was extracted using a maxiprep kit (Invitrogen). The insertion of the sgRNA was confirmed via Sanger sequencing (Genewiz) using the following primer: 5' GACTATCATATGCTTACCGT 3'.

Viral production and stereotaxic injections.

All viruses were prepared in-house as described previously (Gore et al., 2013). Table 2 is a comprehensive list of all viruses used in this study.

Table 2	
1	AAV1-FLEX-SaCas9-sgTh
2	AAV1-FLEX(1loxP)-SaCas9-sgTh
3	AAV1-FLEX-SaCas9-sg*Gt(Rosa26)Sor*
4	AAV1-FLEX-SaCas9-sgKcnn3
5	AAV1-FLEX-SaCas9-sgTh(2)
6	AAV1-FLEX-SaCas9-sgGabrg2
7	AAV1-FLEX-SaCas9-sgGabrg2TTT
8	AAV1-FLEX-SaCas9-sgSlc6a3
9	AAV1-FLEX-SaCas9-sgSlc6a3TTT
10	AAV1-FLEX-SaCas9-sgGrin1
11	AAV1-FLEX-SaCas9-sgGrin1ATG
12	AAV1-FLEX-SaCas9-sgSlc17a7
13	AAV1-FLEX-SaCas9-sgSlc17a6

14	AAV1-FLEX-SaCas9-sgSlc32a1
15	AAV1-hSyn-SpCas9
16	AAV1-U6-sgTh(SpCas9)-hSyn-EGFP-KASH
17	AAV1-FLEX-EGFP-KASH
18	AAV1-FLEXfrt-EGFP-KASH
19	AAV1-FLEX-mCherry
20	AAV1-FLEXfrt-mCherry
21	AAV1-FLEX-ChR2-EYFP

All CRISPR/SaCas9 viruses were made using sereotype AAV1 packaging vector with AAV2 ITRs. The AAV1-FLEX-EGFP-KASH and AAV1-FLEXfrt-EGFP-KASH virus used for FACS and genetic sequencing were synthesized using an AAV1 packaging vector and AAV1 ITRs. The following coordinates were used for stereotaxic viral injections relative to Bregma: VTA (M-L=0.5, A-P=3.25*F, D-V=-4.4, F=(Distance in mm from Bregma to Lambda)/4.21), LPO (M-L=1.0, A-P=0.2, D-V=-5.0), PPTg (M-L=1.2, A-P=-4.5*F, D-V=-3.75), and PFC (M-L=0.3, A-P=2.1, D-V=-2.0).

Basal locomotion and cocaine sensitization.

Standard Allentown cages were placed into locomotion chambers (Columbus instruments) that use infrared beam breaks to calculate distance traveled. For basal locomotion, mice were singly housed in clean cages and provided with ad libitum access to food and water. Locomotion was monitored for 72 consecutive hours. For cocaine sensitization, mice were placed in clean cages with no food or water for 3 hours. Subcutaneous injections of either saline (0.2mL, days 1 and 2) or cocaine (20mg/kg, days 3-7, Sigma-Aldrich) were delivered 90 minutes into the recording session each day for 7 consecutive days.

Slice electrophysiology.

Mice were allowed 3-4 weeks recovery after surgery to allow for viral expression and gene knockout. Horizontal (200 μm) or coronal (250 μm) brain slices were prepared from 8-10 week old mice in an ice slush solution containing (in mM); 92 NMDG, 2.5 KCl, 1.25 NaH_2PO_4, 30 $NaHCO_3$, 20 HEPES, 25 glucose, 2 thiourea, 5 Na-ascorbate, 3 Na-pyruvate, 0.5 $CaCl_2$, 10 $MgSO_4$, pH 7.3–7.4 (Ting et al., 2014). Slices recovered for ~12 min in the same solution at 32°C and then were transferred to a room temperature solution containing (in mM): 92 NaCl, 2.5 KCl, 1.25 NaH_2PO_4, 30 $NaHCO_3$, 20 HEPES, 25 glucose, 2 thiouria, 5 Na-ascorbate, 3 Na-pyruvate, 2 $CaCl_2$, 2 $MgSO_4$. Slices were allowed to recover for an additional 60 minutes. All solutions were continuously bubbled with O_2/CO_2. Whole-cell patch clamp recordings were made using an Axopatch 700B amplifier (Molecular Devices) using 4-6 MΩ electrodes. Recordings were made in ACSF containing (in mM): 126 NaCl, 2.5 KCl, 1.2 NaH_2PO_4, 1.2 $MgCl_2$ 11 D-glucose, 18 $NaHCO_3$, 2.4 $CaCl_2$, at 32°C continually perfused over slices at a rate of ~2 ml/min. VTA dopamine or GABA neurons were identified by fluorescence.

Recording of mIPSCs for sgGabrg2 functional validation. AAV1-FLEX-SaCas9-sgGabrg2 and AAV1-FLEX-EGFP-KASH were coinjected into the VTA of DAT-Cre or Vgat-Cre mice. mIPSC recordings were made in the presence of 2 mM Kynurenic acid (Abcam) and 500 nM Tetrodotoxin (Tocris) to block glutamatergic signaling and action potential firing, respectively. Electrodes were filled with an internal solution containing (in mM): 140 CsCl, 0.2 $CaCl_2$, 8 NaCl, 2 EGTA, 10 HEPES, 1 QX-314, 0.5 Na3GTP, 4 MgATP, pH 7.2, 275-285 mOsm. Cells were held at -60mV and access resistance was monitored throughout the experiment. The mIPSCs were analyzed using Mini Analysis

software (Synaptosoft). The minimum threshfold to count as an mIPSC for amplitude height was 7pA.

Recording of SK currents for sgKcnn3 functional validation. AAV1-FLEX-SaCas9-sgKcnn3 and AAV1-FLEX-mCherry were co-injected into the VTA of DAT-Cre mice. SK currents were measured as described (Soden et al., 2013). Electrodes were filled with an internal solution containing (in mM): 130 K-gluconate, 10 HEPES, 5 NaCl, 1 EGTA, 5 Mg-ATP, 0.5 Na-GTP, pH 7.3, 280 mOsm. Neurons were held at −70 mV in voltage-clamp mode and tail currents were evoked with a 500 ms depolarization to 0 mV. Tail current amplitudes were measured 85 ms after the end of the voltage step, which corresponded with the average time of maximum current in control neurons. Apamin (300 nM, Tocris) was bath applied to a subset of neurons to block SK3 channels.

Recording of AMPA/NMDA currents for sgGrin1 functional validation. AAV1-FLEXfrt-SaCas9-sgGrin1 and AAV1-FLEXfrt-mCherry were co-injected into the VTA of TH-Flp mice. AMPA/NMDA currents were measured as described (Sanford et al., 2017). Picrotoxin (100 uM, Abcam) was included in the bath and electrodes were filled with an internal solution containing (in mM): 120 CsMeSO3, 20 HEPES, 0.4 EGTA, 2.8 NaCl, 2.5 Mg-ATP, 0.25 Na-GTP, 5 QX-314 bromide, pH 7.3, 280 mOsm. Neurons were held at +40 mV while a concentric bipolar electrode placed rostral to the VTA delivered 0.4 ms stimuli at 0.1 Hz to elicit an EPSC containing both AMPA and NMDA components. Approximately 15 traces were averaged per cell, followed by bath application of AP5 (100 μM, Abcam) to isolate the AMPA component. 15 AMPA EPSC traces were

averaged and digitally subtracted from the initial recording in order to generate the NMDA trace.

Recording of light-evoked EPSCs/IPSCs for sgSlc17a7. sgSlc17a6, and Slc32a1 functional validation. Slc17a7 (Vglut1): AAV1-FLEX-ChR2-YFP was co-injected into the PFC along with either AAV1-FLEX-SaCas9-sgSlc17a7 or AAV1-FLEX-SaCas9-sgGt(Rosa26)Sor. Recordings were made from areas of dense ChR2 fiber innervation in the centromedian thalamic nucleus. *Slc17a6* (Vglut2): AAV1-FLEX-ChR2-YFP was co-injected into the PPTg along with either AAV1-FLEX-SaCas9-sgSlc17a6 or AAV1-FLEX-SaCas9-sgGt(Rosa26)Sor. Recordings were made from the VTA. *Slc32a1* (Vgat): AAV1-FLEX-ChR2-YFP was co-injected into the LPO along with either AAV1-FLEX-SaCas9-sgSlc32a1 or AAV1-FLEX-SaCas9-sgGt(Rosa26)Sor. AAV1-FLEX-mCherry was injected into the VTA. Recordings were made from mCherry-labeled (Vgat+) neurons in the VTA.

Light-evoked synaptic transmission was induced with 5 ms light pulses delivered at 0.1 Hz from an optic fiber placed directly in the bath. Amplitudes were calculated from an average of at least 10 events. Light-evoked EPSCs were measured while holding at -60 mV in the presence of picrotoxin (100 µM), with an internal recording solution containing (in mM): 130 K-gluconate, 10 HEPES, 5 NaCl, 1 EGTA, 5 Mg-ATP, 0.5 Na-GTP, 5 QX-314, pH 7.3, 280 mOsm. Light-evoked IPSCs were measured with holding at -60 mV in the presence of kynureinc acid (2 mM) with an internal recording solution containing (in mM): 135 KCl, 12 NaCl, 0.5 EGTA, 10 HEPES, 2.5 Mg-ATP, 0.25 Na-GTP, 5 QX-314, pH 7.3, 280 mOsm.

Immunohistochemistry.

Mice were anesthetized with Beuthanasia (Merck Sharp and Dohme Corp) and perfused transcardially with ice-cold phosphate-buffered saline (PBS) followed by 4% paraformaldehyde (PFA). The brain was removed and placed in 4% PFA overnight, then transferred to 30% sucrose in PBS for 2-3 days. Brains were mounted in OCT (Fisher) at -19˚C and frozen sections (30µm) were cut using a cryostat (Leica). The following primary antibodies were used for protein detection: Tyrosine hydroxylase (mouse monoclonal, 1:2000, Millipore or rabbit polyclonal, 1:2000, Fisher Scientific), GFP (rabbit polyclonal, 1:2000, Invitrogen or chicken polyclonal, 1:6000, Abcam), HA (rabbit polyclonal, 1:2000, Sigma). The slices were first blocked in 1xTBS with 0.3% Triton and 3% normal donkey serum (TBST+NDS). Slices were incubated in primary antibody diluted in TBST+NDS overnight at 4˚C overnight. The following day, brain sections were washed 3x in TBST and then incubated with secondary antibodies (Jackson immuno, Alexa Fluor-488; Cy3) diluted 1:250 in TBST+NDS and then washed 3x times and mounted onto slides using Fluoromount (Southern Biotech). Fluorescence was imaged using a Nikon Upright Widefield microscope, and cells were counted using ImageJ.

Protein isolation.

Mice were allowed 5-8 weeks for recovery and viral expression after surgery. Tissue punches of the ventral midbrain or ventral striatum were flash frozen in liquid nitrogen and then homogenized in 10mM HEPES pH 7.4 with 0.1mM PIC (Sigma) using glass dounces (25x with dounce A, 25x with dounce B). The homogenate was centrifuged at

1000xg for 10min at 4˚C. The supernatant was removed and centrifuged at 14000RPM for 20min at 4˚C. The protein pellet was vigorously resuspended in RIPPA lysis buffer containing (in mM): 50 Tris pH 7.4, 150 NaCl, 0.1% SDS, 0.5% Na-Deoxycholate, 1% NP-40, 0.1mM PIC and rotated at 4˚C for 1 hour. The protein suspension was centrifuged at 14000RPM for 15min at 4˚C to pellet any insoluble material. The supernatant was resuspended in 6x sample buffer containing: 6.3% SDS, 60% glycerol, 374mM Tris Base, 5.5% β-mercaptoethanol, 0.67% Bromo Blue, and stored at -80˚C.

Western blot.

Protein samples were denatured at 100˚C for 5min before loaded in a 10% precast polyacrylamide gel (Biorad) and run at 80mV for ~1.5hours in running buffer containing (in mM): 25 Tris base, 192 glycine and 0.1% SDS. Protein was transferred from the gel to a PVDF membrane via electrophoresis in transfer buffer containing (in mM) 25 Tris base, 192 glycine and 20% methanol. The membranes were incubated in blocking buffer containing (in mM): 10mM Tris pH 7.4, 100mM NaCl, 0.1% Tween 20, and 5% dehydrated milk for 30min at room temperature. The membranes were incubated in the following primary antibodies overnight at 4˚C with rotation: Tyrosine Hydroxylase (rabbit polyclonal, 1:10,000, Millipore), Actin (mouse monoclonal, 1:10,000), Dopamine Transporter (rat polyclonal, 1:2000, Millipore). The blots were washed 3x in wash buffer containing (in mM): 10mM Tris pH 7.4, 100mM NaCl, and 0.1% Tween 20, and incubated in 1:5000 secondary antibody conjugated to HRP for 2 hours (goat anti-rabbit, goat anti-mouse, goat anti-rat, Abcam). The blots were washed 3x in wash buffer, and

incubated for 5min in ECL Western Blotting Substrate (Thermo Fisher) to expose the protein. Protein levels were quantified using ImageJ.

Nuclear isolation and FACS.

The tissue punches of individual mice within an experimental or control group were combined (3 mice/group). Tissue punches of the ventral midbrain were flash frozen in liquid nitrogen for later use or directly homogenized in 2mL of homogenization buffer containing (in mM): 320 Sucrose (sterile filtered), 5 CaCl (sterile filtered), 3 Mg(Ac)2 (sterile filtered), 10 Tris pH 7.8 (sterile filtered), 0.1 EDTA pH 8 (sterile filtered), 0.1% NP40, 0.1 Protease Inhibitor Cocktail (PIC, Sigma), 1 β-mercaptoethanol according to Swiech et al 2014. Sterile filtration was performed using 0.45μm syringe filters (Millipore). The volume was then brought up to 5mL using homogenization buffer and was incubated on ice for 5 minutes. For centrifugation, 5mL of 50% Optiprep density gradient medium (Sigma) containing (in mM): 5 CaCl (sterile filtered), 3 Mg(Ac)2 (sterile filtered), 10 Tris pH 7.8 (sterile filtered), 0.1 PIC, 1 β-mercaptoethanol was added to the homogenate and mixed by inversion. The mixture was gently loaded on 10mL of 29% iso-osmolar Optiprep solution in a 1x3 ½ in Beckman centrifuge tube (SW32 Ti rotor) and spun at 7500 RPM for 30min at 4˚C. The cell debris was removed using a KimWipe and the supernatant was gently poured out. The nuclei pellet was vigorously resuspended in sterile 1xPBS and immediately taken to be further processed.

Generation of amplicons.

GFP-positive nuclei were sorted using a BD AriaFACS III into a PCR tube strip containing REPLI-g Advanced Single Cell Storage buffer (Qiagen). Whole genome amplification (WGA) was performed on the samples directly following FACS using the REPLI-g Advanced DNA Single Cell kit (Qiagen) according to manufacturer's instructions.

For generation of the specific amplicons, 1ul of WGA DNA was diluted 1:50 and amplified (PCR 1, see Table 5 for primers) with Phusion High Fidelity Polymerase (Thermo Fisher) using the thermocycler protocol in Table 3.

Table 3

Step		**Phase**	**Time (sec)**	**Temperature (°C)**
1		Initial denaturation	30	95
2	x34	Denaturation	10	95
3		Annealing	20	64
4		Extension	10	72
5		Final Extension	5	72
6		Hold	Forever	12

The product of PCR 1 was diluted 1:100 and amplified again (PCR 2) with a second set of primers (Table 5) to decrease non-specific amplification and increase amplified DNA yield using the thermocycler protocol in Table 3. The amplicons were gel extracted using the MinElute gel extraction kit (Qiagen), and stored at 20°C or directly used in downstream processing.

T7E1 Assay.

The T7 endonuclease 1 (T7E1) assay was performed on amplicons spanning targeted regions. A 10uL reaction including 150ng of amplicons, 1uL of NEB Buffer 2 and water was placed into a thermocycler using the protocol in Table 4. 1uL of T7E1 was added to

each sample and placed in 37°C water bath for 15min. Samples were run on a 2% agarose gel.

Table 4			
Phase	**Time (min)**	**Temperature (˚C)**	**Ramp rate**
Initial denaturation	5	95	
Annealing	95-85˚C		-2˚C/sec
	85-25˚C		-0.1˚C/sec
Hold	Forever	4	

Sequencing.

For exome sequencing, 500ng of WGA genomic DNA from GFP+ sorted nuclei was sent to Genewiz on dry ice. Samples were processed using the Genewiz standardized workflow of fragmentation, library prep, hybridization, PCR amplification, and sequencing using Illumina HiSeq 2X150PE. Sequences were referenced to the mouse reference genome *Mus musculus* mm9. The following barcode sequences were used, Rosa26-GFP(+): AGATGTAC, TH-GFP(+): CCGAATA, Rosa26-GFP(-): CCATCCTC, and TH-GFP(-): TCTTCACA. Total reads after adapter trimming and percent greater than 20X coverage was, Rosa26-GFP(+): 218,032,474; 82.05%, TH-GFP(+): 215,568,918; 93.94%, Rosa26-GFP(-): 199,822,240; 81.54%, and TH-GFP(-): 192,337,296; 97.67%.

For both targeted deep sequencing (Amplicon EZ) and Sanger Sequencing, amplicons were sent to Genewiz. Amplicons ranged in size from ~170bp to ~450bp. Differences in amplicon size was required due to the unique sequence architecture of each gene. All Sanger sequencing was completed using the primer in the same direction as the sgRNA except for sgSlc17a7. A large G-C rich region just upstream of the sgRNA-targeted region inhibited PCR amplification. Therefore, amplification primers

were required to be designed downstream of the G-C rich region, leaving only 47 bp between the 5' end of the forward primer and the SaCas9 cleavage site. 47 bp is too close to the modified region to obtain Sanger sequencing results of the mutations, therefore, the reverse primer was used instead.

Table 5

Gene	PCR #	Primers
Th	1	Forward: 5' TTGTGCTCCTACAGTCTCTGG 3' Reverse: 5' ACATATCTTATGCATGCTACC 3'
	2	Forward: 5' TTCCAGTTCTGCCATGGCTCT 3' Reverse: 5' ACATATCTTATGCATGCTACC 3'
Gt(Rosa26)Sor	1	Forward: 5' AAAGTCGCTCTGAGTTGTTATCAG 3' Reverse: 5' GGAGCGGGAGAAATGGATATG 3'
	2	Forward: 5' AAAGGCTAACCTGGTGTGTGG 3' Reverse: 5' GGAGCGGGAGAAATGGATATG 3'
Gabrg2	1	Forward: 5' GGCATCAAATCATCAGCATA 3' Reverse: 5' TATGAAACGAGCTTAAGCTC 3'
	2	Forward: 5' GGCATCAAATCATCAGCATA 3' Reverse: 5' TCTCAAATCTGGGTGGTCTC 3'
Slc6a3	1	Forward: 5' CTCTAGACATGTCTACTGAAT 3' Reverse: 5' TGTAGCACAGGTAGGGAAACC 3'
	2	Forward: 5' CTCTAGACATGTCTACTGAAT 3' Reverse: 5' GATGACTGAGAGCAGGAA 3'
Slc17a7	1	Forward: 5' GGATTGGCAGGGGAC 3' Reverse: 5' ACATTGTGCCTGGGTGTCGCC3'
	2	Forward: 5' GGATTGGCAGGGGAC 3' Reverse: 5' CCTCTGTCAGTTGCTCTCAGA 3'
Slc17a6	1	Forward: 5' CTTAAATTGACCTGAGGAGGC 3' Reverse: 5' TGCAGTACAGTTAATACCTAC 3'
	2	Forward: 5' CTTAAATTGACCTGAGGAGGC 3' Reverse: 5' TCAATTGCACCCAAACTTGAC 3'
Slc32a1	1	Forward: 5' CGCAGCAAGCTGACCAATGTG 3' Reverse: 5' GAGCCTGGCAAGGACAGCTCA 3'
	2	Forward: 5' CGCAGCAAGCTGACCAATGTG 3' Reverse: 5' ACTCACCTGAATGGCAT 3'
Grin1	1	Forward: 5' CAATACGCTTCAGCACCTCGG 3' Reverse: 5' AGGAAGTAGTGGTCACCTGGC 3'
	2	Forward: 5' CAATACGCTTCAGCACCTCGG 3' Reverse: 5' GCTTGTGGGTGACAGAAGTG 3'
Kcnn3	1	Forward: 5' CAATGCATACTCGAGTGGCAG 3' Reverse: 5' GACAAGCTGGCTCTGGAGTTG 3'
	2	Forward: 5' CAATGCATACTCGAGTGGCAG 3'

		Reverse: 5’ TGCTGCGACTGTTGCTGCTGA 3’
Paxbp1	1	Forward: 5’ CTTCTCACCTGGACTCCTCTT 3’ Reverse: 5’ ACACTAGGCACATCTGAAAGC 3’
	2	Forward: 5’ CTTCTCACCTGGACTCCTCTT 3’ Reverse: 5’ CCACGTGCTGAGCC 3’
Socs6	1	Forward: 5’ GACTGAGTTCTCAGATGTGTC 3’ Reverse: 5’ CCTGACCTGGTCTGCCAAATG 3’
	2	Forward: 5’ GACTGAGTTCTCAGATGTGTC 3’ Reverse: 5’ ATGTAGAGCTATGACTG 3’
Wdfy3	1	Forward: 5’ GAAGGAAGTAGGAAAGAGGAA 3’ Reverse: 5’ ACGGGCTGCTCCTCTCCATCAA 3’
	2	Forward: 5’ GAAGGAAGTAGGAAAGAGGAA 3’ Reverse: 5’ AACATCCCGGAAAGTGAG 3’
Ndn	1	Forward: 5’ CGAAGAACGGATAGAAGATGT 3’ Reverse: 5’ TCACATAGATGAGGCTCAGGA 3’
	2	Forward: 5’ CGAAGAACGGATAGAAGATGT 3’ Reverse: 5’ GATTGGTCAGCCTCAGGTGCA 3’

ACKNOWLEDGMENTS

First, thank you to Christopher, my family, and my friends for the endless support. You mean everything to me.

Thank you to everyone who contributed to the studies in this paper, I could not have completed this without you. Thank you especially to my mentor Dr. Larry Zweifel: those 10am Monday meetings were critical to my success. And thank you to Dr. Richard Palmiter: I value your guidance (and sense of humor) immensely. I am also thankful for scientific advice (and companionship) from the Zweifel lab. May HHH always exist.

REFERENCES

1. Aird, E.J., Lovendahl, K.N., St Martin, A., Harris, R.S., and Gordon, W.R. (2018). Increasing Cas9-mediated homology-directed repair efficiency through covalent tethering of DNA repair template. Communications biology *1*, 54.
2. Andersson, A.F., and Banfield, J.F. (2008). Virus population dynamics and acquired virus resistance in natural microbial communities. Science *320*, 1047-1050.
3. Anzalone, A.V., Randolph, P.B., Davis, J.R., Sousa, A.A., Koblan, L.W., Levy, J.M., Chen, P.J., Wilson, C., Newby, G.A., Raguram, A.*, et al.* (2019). Search-and-replace genome editing without double-strand breaks or donor DNA. Nature.
4. Back, S., Necarsulmer, J., Whitaker, L.R., Coke, L.M., Koivula, P., Heathward, E.J., Fortuno, L.V., Zhang, Y., Yeh, C.G., Baldwin, H.A.*, et al.* (2019). Neuron-Specific Genome Modification in the Adult Rat Brain Using CRISPR-Cas9 Transgenic Rats. Neuron.
5. Barrangou, R., Fremaux, C., Deveau, H., Richards, M., Boyaval, P., Moineau, S., Romero, D.A., and Horvath, P. (2007). CRISPR provides acquired resistance against viruses in prokaryotes. Science *315*, 1709-1712.
6. Bocklisch, C., Pascoli, V., Wong, J.C., House, D.R., Yvon, C., de Roo, M., Tan, K.R., and Luscher, C. (2013). Cocaine disinhibits dopamine neurons by potentiation of GABA transmission in the ventral tegmental area. Science *341*, 1521-1525.
7. Bolotin, A., Quinquis, B., Sorokin, A., and Ehrlich, S.D. (2005). Clustered regularly interspaced short palindrome repeats (CRISPRs) have spacers of extrachromosomal origin. Microbiology *151*, 2551-2561.
8. Bondy-Denomy, J., Pawluk, A., Maxwell, K.L., and Davidson, A.R. (2013). Bacteriophage genes that inactivate the CRISPR/Cas bacterial immune system. Nature *493*, 429-432.
9. Bult, C.J., Blake, J.A., Smith, C.L., Kadin, J.A., and Richardson, J.E. (2019). Mouse Genome Database (MGD) 2019. Nucleic acids research *47*, D801-D806.
10. Cameron, D.L., and Williams, J.T. (1994). Cocaine inhibits GABA release in the VTA through endogenous 5-HT. The Journal of neuroscience : the official journal of the Society for Neuroscience *14*, 6763-6767.
11. Carlson-Stevermer, J., Abdeen, A.A., Kohlenberg, L., Goedland, M., Molugu, K., Lou, M., and Saha, K. (2017). Assembly of CRISPR ribonucleoproteins with biotinylated oligonucleotides via an RNA aptamer for precise gene editing. Nature communications *8*, 1711.
12. Chaudhry, F.A., Reimer, R.J., Bellocchio, E.E., Danbolt, N.C., Osen, K.K., Edwards, R.H., and Storm-Mathisen, J. (1998). The vesicular GABA transporter, VGAT, localizes to synaptic vesicles in sets of glycinergic as well as GABAergic neurons. The Journal of neuroscience : the official journal of the Society for Neuroscience *18*, 9733-9750.
13. Chen, R.Z., Akbarian, S., Tudor, M., and Jaenisch, R. (2001). Deficiency of methyl-CpG binding protein-2 in CNS neurons results in a Rett-like phenotype in mice. Nature genetics *27*, 327-331.

14. Coic, E., Feldman, T., Landman, A.S., and Haber, J.E. (2008). Mechanisms of Rad52-independent spontaneous and UV-induced mitotic recombination in Saccharomyces cerevisiae. Genetics *179*, 199-211.
15. Colasante, G., Lignani, G., Brusco, S., Di Berardino, C., Carpenter, J., Giannelli, S., Valassina, N., Bido, S., Ricci, R., Castoldi, V.*, et al.* (2019). dCas9-Based Scn1a Gene Activation Restores Inhibitory Interneuron Excitability and Attenuates Seizures in Dravet Syndrome Mice. Molecular therapy : the journal of the American Society of Gene Therapy.
16. Concordet, J.P., and Haeussler, M. (2018). CRISPOR: intuitive guide selection for CRISPR/Cas9 genome editing experiments and screens. Nucleic acids research *46*, W242-W245.
17. Cong, L., Ran, F.A., Cox, D., Lin, S., Barretto, R., Habib, N., Hsu, P.D., Wu, X., Jiang, W., Marraffini, L.A.*, et al.* (2013). Multiplex genome engineering using CRISPR/Cas systems. Science *339*, 819-823.
18. Darvas, M., and Palmiter, R.D. (2010). Restricting dopaminergic signaling to either dorsolateral or medial striatum facilitates cognition. The Journal of neuroscience : the official journal of the Society for Neuroscience *30*, 1158-1165.
19. Deignan, J., Lujan, R., Bond, C., Riegel, A., Watanabe, M., Williams, J.T., Maylie, J., and Adelman, J.P. (2012). SK2 and SK3 expression differentially affect firing frequency and precision in dopamine neurons. Neuroscience *217*, 67-76.
20. Deleye, L., Tilleman, L., Vander Plaetsen, A.S., Cornelis, S., Deforce, D., and Van Nieuwerburgh, F. (2017). Performance of four modern whole genome amplification methods for copy number variant detection in single cells. Scientific reports *7*, 3422.
21. Dravet, C. (2011). The core Dravet syndrome phenotype. Epilepsia *52 Suppl 2*, 3-9.
22. Edwards, N.J., Tejeda, H.A., Pignatelli, M., Zhang, S., McDevitt, R.A., Wu, J., Bass, C.E., Bettler, B., Morales, M., and Bonci, A. (2017). Corrigendum: Circuit specificity in the inhibitory architecture of the VTA regulates cocaine-induced behavior. Nature neuroscience *20*, 1189.
23. Engblom, D., Bilbao, A., Sanchis-Segura, C., Dahan, L., Perreau-Lenz, S., Balland, B., Parkitna, J.R., Lujan, R., Halbout, B., Mameli, M.*, et al.* (2008). Glutamate receptors on dopamine neurons control the persistence of cocaine seeking. Neuron *59*, 497-508.
24. Fernandes, L.G.V., Guaman, L.P., Vasconcellos, S.A., Heinemann, M.B., Picardeau, M., and Nascimento, A. (2019). Gene silencing based on RNA-guided catalytically inactive Cas9 (dCas9): a new tool for genetic engineering in Leptospira. Scientific reports *9*, 1839.
25. Fremeau, R.T., Jr., Troyer, M.D., Pahner, I., Nygaard, G.O., Tran, C.H., Reimer, R.J., Bellocchio, E.E., Fortin, D., Storm-Mathisen, J., and Edwards, R.H. (2001). The expression of vesicular glutamate transporters defines two classes of excitatory synapse. Neuron *31*, 247-260.
26. Fu, Y., Foden, J.A., Khayter, C., Maeder, M.L., Reyon, D., Joung, J.K., and Sander, J.D. (2013). High-frequency off-target mutagenesis induced by CRISPR-Cas nucleases in human cells. Nature biotechnology *31*, 822-826.
27. Fuchsbauer, O., Swuec, P., Zimberger, C., Amigues, B., Levesque, S., Agudelo, D., Duringer, A., Chaves-Sanjuan, A., Spinelli, S., Rousseau, G.M.*, et al.* (2019). Cas9 Allosteric Inhibition by the Anti-CRISPR Protein AcrIIA6. Molecular cell.

28. Garneau, J.E., Dupuis, M.E., Villion, M., Romero, D.A., Barrangou, R., Boyaval, P., Fremaux, C., Horvath, P., Magadan, A.H., and Moineau, S. (2010). The CRISPR/Cas bacterial immune system cleaves bacteriophage and plasmid DNA. Nature *468*, 67-71.
29. Gilbert, L.A., Larson, M.H., Morsut, L., Liu, Z., Brar, G.A., Torres, S.E., Stern-Ginossar, N., Brandman, O., Whitehead, E.H., Doudna, J.A.*, et al.* (2013). CRISPR-mediated modular RNA-guided regulation of transcription in eukaryotes. Cell *154*, 442-451.
30. Giros, B., Jaber, M., Jones, S.R., Wightman, R.M., and Caron, M.G. (1996). Hyperlocomotion and indifference to cocaine and amphetamine in mice lacking the dopamine transporter. Nature *379*, 606-612.
31. Gore, B.B., Soden, M.E., and Zweifel, L.S. (2013). Manipulating gene expression in projection-specific neuronal populations using combinatorial viral approaches. Current protocols in neuroscience *65*, 4 35 31-20.
32. Grieger, J.C., and Samulski, R.J. (2005). Packaging capacity of adeno-associated virus serotypes: impact of larger genomes on infectivity and postentry steps. Journal of virology *79*, 9933-9944.
33. Haeussler, M., Schonig, K., Eckert, H., Eschstruth, A., Mianne, J., Renaud, J.B., Schneider-Maunoury, S., Shkumatava, A., Teboul, L., Kent, J.*, et al.* (2016). Evaluation of off-target and on-target scoring algorithms and integration into the guide RNA selection tool CRISPOR. Genome biology *17*, 148.
34. Hasegawa, Y., Daitoku, Y., Sekiguchi, K., Tanimoto, Y., Mizuno-Iijima, S., Mizuno, S., Kajiwara, N., Ema, M., Miwa, Y., Mekada, K.*, et al.* (2013). Novel ROSA26 Cre-reporter knock-in C57BL/6N mice exhibiting green emission before and red emission after Cre-mediated recombination. Experimental animals *62*, 295-304.
35. Ishino, Y., Krupovic, M., and Forterre, P. (2018). History of CRISPR-Cas from Encounter with a Mysterious Repeated Sequence to Genome Editing Technology. Journal of bacteriology *200*.
36. Ishino, Y., Shinagawa, H., Makino, K., Amemura, M., and Nakata, A. (1987). Nucleotide sequence of the iap gene, responsible for alkaline phosphatase isozyme conversion in Escherichia coli, and identification of the gene product. Journal of bacteriology *169*, 5429-5433.
37. Jansen, R., Embden, J.D., Gaastra, W., and Schouls, L.M. (2002). Identification of genes that are associated with DNA repeats in prokaryotes. Molecular microbiology *43*, 1565-1575.
38. Jiang, F., and Doudna, J.A. (2017). CRISPR-Cas9 Structures and Mechanisms. Annual review of biophysics *46*, 505-529.
39. Jiang, F., Zhou, K., Ma, L., Gressel, S., and Doudna, J.A. (2015). STRUCTURAL BIOLOGY. A Cas9-guide RNA complex preorganized for target DNA recognition. Science *348*, 1477-1481.
40. Jinek, M., Chylinski, K., Fonfara, I., Hauer, M., Doudna, J.A., and Charpentier, E. (2012). A programmable dual-RNA-guided DNA endonuclease in adaptive bacterial immunity. Science *337*, 816-821.
41. Kalivas, P.W., and Stewart, J. (1991). Dopamine transmission in the initiation and expression of drug- and stress-induced sensitization of motor activity. Brain research Brain research reviews *16*, 223-244.

42. Kelkar, A., Zhu, Y., Groth, T., Stolfa, G., Stablewski, A.B., Singhi, N., Nemeth, M., and Neelamegham, S. (2019). Doxycycline-Dependent Self-Inactivation of CRISPR-Cas9 to Temporally Regulate On- and Off-Target Editing. Molecular therapy : the journal of the American Society of Gene Therapy.
43. Kent, W.J., Sugnet, C.W., Furey, T.S., Roskin, K.M., Pringle, T.H., Zahler, A.M., and Haussler, D. (2002). The human genome browser at UCSC. Genome research *12*, 996-1006.
44. Kim, D., Bae, S., Park, J., Kim, E., Kim, S., Yu, H.R., Hwang, J., Kim, J.I., and Kim, J.S. (2015). Digenome-seq: genome-wide profiling of CRISPR-Cas9 off-target effects in human cells. Nature methods *12*, 237-243, 231 p following 243.
45. Kim, E., Koo, T., Park, S.W., Kim, D., Kim, K., Cho, H.Y., Song, D.W., Lee, K.J., Jung, M.H., Kim, S.*, et al.* (2017). In vivo genome editing with a small Cas9 orthologue derived from Campylobacter jejuni. Nature communications *8*, 14500.
46. Kumar, N., Stanford, W., de Solis, C., Aradhana, Abraham, N.D., Dao, T.J., Thaseen, S., Sairavi, A., Gonzalez, C.U., and Ploski, J.E. (2018). The Development of an AAV-Based CRISPR SaCas9 Genome Editing System That Can Be Delivered to Neurons in vivo and Regulated via Doxycycline and Cre-Recombinase. Frontiers in molecular neuroscience *11*, 413.
47. Lammel, S., Lim, B.K., and Malenka, R.C. (2014). Reward and aversion in a heterogeneous midbrain dopamine system. Neuropharmacology *76 Pt B*, 351-359.
48. Larson, M.H., Gilbert, L.A., Wang, X., Lim, W.A., Weissman, J.S., and Qi, L.S. (2013). CRISPR interference (CRISPRi) for sequence-specific control of gene expression. Nature protocols *8*, 2180-2196.
49. Liu, Q.S., Pu, L., and Poo, M.M. (2005). Repeated cocaine exposure in vivo facilitates LTP induction in midbrain dopamine neurons. Nature *437*, 1027-1031.
50. Lusby, E., Fife, K.H., and Berns, K.I. (1980). Nucleotide sequence of the inverted terminal repetition in adeno-associated virus DNA. Journal of virology *34*, 402-409.
51. Makarova, K.S., and Koonin, E.V. (2015). Annotation and Classification of CRISPR-Cas Systems. Methods Mol Biol *1311*, 47-75.
52. Mali, P., Yang, L., Esvelt, K.M., Aach, J., Guell, M., DiCarlo, J.E., Norville, J.E., and Church, G.M. (2013). RNA-guided human genome engineering via Cas9. Science *339*, 823-826.
53. Mekler, V., Minakhin, L., and Severinov, K. (2017). Mechanism of duplex DNA destabilization by RNA-guided Cas9 nuclease during target interrogation. Proceedings of the National Academy of Sciences of the United States of America *114*, 5443-5448.
54. Mohammadparast, S., Bayat, H., Biglarian, A., and Ohadi, M. (2014). Exceptional expansion and conservation of a CT-repeat complex in the core promoter of PAXBP1 in primates. American journal of primatology *76*, 747-756.
55. Mojica, F.J., Diez-Villasenor, C., Garcia-Martinez, J., and Soria, E. (2005). Intervening sequences of regularly spaced prokaryotic repeats derive from foreign genetic elements. Journal of molecular evolution *60*, 174-182.
56. Mojica, F.J., Diez-Villasenor, C., Soria, E., and Juez, G. (2000). Biological significance of a family of regularly spaced repeats in the genomes of Archaea, Bacteria and mitochondria. Molecular microbiology *36*, 244-246.

57. Morales, M., and Margolis, E.B. (2017). Ventral tegmental area: cellular heterogeneity, connectivity and behaviour. Nature reviews Neuroscience *18*, 73-85.
58. Muzyczka, N., Samulski, R.J., Hermonat, P., Srivastava, A., and Berns, K.I. (1984). The genetics of adeno-associated virus. Advances in experimental medicine and biology *179*, 151-161.
59. Nishimasu, H., Cong, L., Yan, W.X., Ran, F.A., Zetsche, B., Li, Y., Kurabayashi, A., Ishitani, R., Zhang, F., and Nureki, O. (2015). Crystal Structure of Staphylococcus aureus Cas9. Cell *162*, 1113-1126.
60. Nishimasu, H., Ran, F.A., Hsu, P.D., Konermann, S., Shehata, S.I., Dohmae, N., Ishitani, R., Zhang, F., and Nureki, O. (2014). Crystal structure of Cas9 in complex with guide RNA and target DNA. Cell *156*, 935-949.
61. Nishiyama, J., Mikuni, T., and Yasuda, R. (2017). Virus-Mediated Genome Editing via Homology-Directed Repair in Mitotic and Postmitotic Cells in Mammalian Brain. Neuron *96*, 755-768 e755.
62. Parker, J.G., Wanat, M.J., Soden, M.E., Ahmad, K., Zweifel, L.S., Bamford, N.S., and Palmiter, R.D. (2011). Attenuating GABA(A) receptor signaling in dopamine neurons selectively enhances reward learning and alters risk preference in mice. The Journal of neuroscience : the official journal of the Society for Neuroscience *31*, 17103-17112.
63. Pawluk, A., Staals, R.H., Taylor, C., Watson, B.N., Saha, S., Fineran, P.C., Maxwell, K.L., and Davidson, A.R. (2016). Inactivation of CRISPR-Cas systems by anti-CRISPR proteins in diverse bacterial species. Nature microbiology *1*, 16085.
64. Platt, R.J., Chen, S., Zhou, Y., Yim, M.J., Swiech, L., Kempton, H.R., Dahlman, J.E., Parnas, O., Eisenhaure, T.M., Jovanovic, M.*, et al.* (2014). CRISPR-Cas9 knockin mice for genome editing and cancer modeling. Cell *159*, 440-455.
65. Poulin, J.F., Caronia, G., Hofer, C., Cui, Q., Helm, B., Ramakrishnan, C., Chan, C.S., Dombeck, D.A., Deisseroth, K., and Awatramani, R. (2018). Mapping projections of molecularly defined dopamine neuron subtypes using intersectional genetic approaches. Nature neuroscience *21*, 1260-1271.
66. Pourcel, C., Salvignol, G., and Vergnaud, G. (2005). CRISPR elements in Yersinia pestis acquire new repeats by preferential uptake of bacteriophage DNA, and provide additional tools for evolutionary studies. Microbiology *151*, 653-663.
67. Qi, L.S., Larson, M.H., Gilbert, L.A., Doudna, J.A., Weissman, J.S., Arkin, A.P., and Lim, W.A. (2013). Repurposing CRISPR as an RNA-guided platform for sequence-specific control of gene expression. Cell *152*, 1173-1183.
68. Ran, F.A., Cong, L., Yan, W.X., Scott, D.A., Gootenberg, J.S., Kriz, A.J., Zetsche, B., Shalem, O., Wu, X., Makarova, K.S.*, et al.* (2015). In vivo genome editing using Staphylococcus aureus Cas9. Nature *520*, 186-191.
69. Ran, F.A., Hsu, P.D., Wright, J., Agarwala, V., Scott, D.A., and Zhang, F. (2013). Genome engineering using the CRISPR-Cas9 system. Nature protocols *8*, 2281-2308.
70. Russell, D.W., and Hirata, R.K. (1998). Human gene targeting by viral vectors. Nature genetics *18*, 325-330.
71. Sadowski, P.D. (1995). The Flp recombinase of the 2-microns plasmid of Saccharomyces cerevisiae. Progress in nucleic acid research and molecular biology *51*, 53-91.

72. Saito, Y.C., Tsujino, N., Hasegawa, E., Akashi, K., Abe, M., Mieda, M., Sakimura, K., and Sakurai, T. (2013). GABAergic neurons in the preoptic area send direct inhibitory projections to orexin neurons. Frontiers in neural circuits *7*, 192.
73. Salvatore, M.F., Calipari, E.S., and Jones, S.R. (2016). Regulation of Tyrosine Hydroxylase Expression and Phosphorylation in Dopamine Transporter-Deficient Mice. ACS chemical neuroscience *7*, 941-951.
74. Sanford, C.A., Soden, M.E., Baird, M.A., Miller, S.M., Schulkin, J., Palmiter, R.D., Clark, M., and Zweifel, L.S. (2017). A Central Amygdala CRF Circuit Facilitates Learning about Weak Threats. Neuron *93*, 164-178.
75. Sarpal, D., Koenig, J.I., Adelman, J.P., Brady, D., Prendeville, L.C., and Shepard, P.D. (2004). Regional distribution of SK3 mRNA-containing neurons in the adult and adolescent rat ventral midbrain and their relationship to dopamine-containing cells. Synapse *53*, 104-113.
76. Schweizer, C., Balsiger, S., Bluethmann, H., Mansuy, I.M., Fritschy, J.M., Mohler, H., and Luscher, B. (2003). The gamma 2 subunit of GABA(A) receptors is required for maintenance of receptors at mature synapses. Molecular and cellular neurosciences *24*, 442-450.
77. Sharon, E., Chen, S.A., Khosla, N.M., Smith, J.D., Pritchard, J.K., and Fraser, H.B. (2018). Functional Genetic Variants Revealed by Massively Parallel Precise Genome Editing. Cell *175*, 544-557 e516.
78. Shepard, P.D., and Bunney, B.S. (1991). Repetitive firing properties of putative dopamine-containing neurons in vitro: regulation by an apamin-sensitive Ca(2+)-activated K+ conductance. Experimental brain research *86*, 141-150.
79. Soden, M.E., Jones, G.L., Sanford, C.A., Chung, A.S., Guler, A.D., Chavkin, C., Lujan, R., and Zweifel, L.S. (2013). Disruption of dopamine neuron activity pattern regulation through selective expression of a human KCNN3 mutation. Neuron *80*, 997-1009.
80. Song, A.J., and Palmiter, R.D. (2018). Detecting and Avoiding Problems When Using the Cre-lox System. Trends in genetics : TIG *34*, 333-340.
81. Soriano, P. (1999). Generalized lacZ expression with the ROSA26 Cre reporter strain. Nature genetics *21*, 70-71.
82. Srinivas, S., Watanabe, T., Lin, C.S., William, C.M., Tanabe, Y., Jessell, T.M., and Costantini, F. (2001). Cre reporter strains produced by targeted insertion of EYFP and ECFP into the ROSA26 locus. BMC developmental biology *1*, 4.
83. Steffensen, S.C., Taylor, S.R., Horton, M.L., Barber, E.N., Lyle, L.T., Stobbs, S.H., and Allison, D.W. (2008). Cocaine disinhibits dopamine neurons in the ventral tegmental area via use-dependent blockade of GABA neuron voltage-sensitive sodium channels. The European journal of neuroscience *28*, 2028-2040.
84. Sternberg, S.H., Redding, S., Jinek, M., Greene, E.C., and Doudna, J.A. (2014). DNA interrogation by the CRISPR RNA-guided endonuclease Cas9. Nature *507*, 62-67.
85. Swiech, L., Heidenreich, M., Banerjee, A., Habib, N., Li, Y., Trombetta, J., Sur, M., and Zhang, F. (2015). In vivo interrogation of gene function in the mammalian brain using CRISPR-Cas9. Nature biotechnology *33*, 102-106.

86. Tervo, D.G., Hwang, B.Y., Viswanathan, S., Gaj, T., Lavzin, M., Ritola, K.D., Lindo, S., Michael, S., Kuleshova, E., Ojala, D.*, et al.* (2016). A Designer AAV Variant Permits Efficient Retrograde Access to Projection Neurons. Neuron *92*, 372-382.
87. Tsai, S.Q., Zheng, Z., Nguyen, N.T., Liebers, M., Topkar, V.V., Thapar, V., Wyvekens, N., Khayter, C., Iafrate, A.J., Le, L.P.*, et al.* (2015). GUIDE-seq enables genome-wide profiling of off-target cleavage by CRISPR-Cas nucleases. Nature biotechnology *33*, 187-197.
88. Wilkinson, R.A., Martin, C., Nemudryi, A.A., and Wiedenheft, B. (2019). CRISPR RNA-guided autonomous delivery of Cas9. Nature structural & molecular biology *26*, 14-24.
89. Wolfart, J., Neuhoff, H., Franz, O., and Roeper, J. (2001). Differential expression of the small-conductance, calcium-activated potassium channel SK3 is critical for pacemaker control in dopaminergic midbrain neurons. The Journal of neuroscience : the official journal of the Society for Neuroscience *21*, 3443-3456.
90. Wu, Z., Yang, H., and Colosi, P. (2010). Effect of genome size on AAV vector packaging. Molecular therapy : the journal of the American Society of Gene Therapy *18*, 80-86.
91. Xie, H., Tang, L., He, X., Liu, X., Zhou, C., Liu, J., Ge, X., Li, J., Liu, C., Zhao, J.*, et al.* (2018). SaCas9 Requires 5'-NNGRRT-3' PAM for Sufficient Cleavage and Possesses Higher Cleavage Activity than SpCas9 or FnCpf1 in Human Cells. Biotechnology journal *13*, e1800080.
92. Zhou, Z., Hong, E.J., Cohen, S., Zhao, W.N., Ho, H.Y., Schmidt, L., Chen, W.G., Lin, Y., Savner, E., Griffith, E.C.*, et al.* (2006). Brain-specific phosphorylation of MeCP2 regulates activity-dependent Bdnf transcription, dendritic growth, and spine maturation. Neuron *52*, 255-269.
93. Zhuang, X., Masson, J., Gingrich, J.A., Rayport, S., and Hen, R. (2005). Targeted gene expression in dopamine and serotonin neurons of the mouse brain. Journal of neuroscience methods *143*, 27-32.
94. Zweifel, L.S., Argilli, E., Bonci, A., and Palmiter, R.D. (2008). Role of NMDA receptors in dopamine neurons for plasticity and addictive behaviors. Neuron *59*, 486-496.